Smart Mater. Struct. 22 (2013) 035003 (17pp) doi:10.1088/0964-1726/22/3/035003

Analyses of functionally graded plates with a magnetoelectroelastic layer

J Sladek[1], V Sladek[1], S Krahulec[1] and E Pan[2]

[1] Institute of Construction and Architecture, Slovak Academy of Sciences, 84503 Bratislava, Slovakia
[2] Department of Civil Engineering, University of Akron, Akron, OH 44325-3905, USA

E-mail: pan2@uakron.edu

Received 7 December 2012
Published 28 January 2013
Online at stacks.iop.org/SMS/22/035003

Abstract

A meshless local Petrov–Galerkin (MLPG) method is presented for the analysis of functionally graded material (FGM) plates with a sensor/actuator magnetoelectroelastic layer localized on the top surface of the plate. The Reissner–Mindlin shear deformation theory is applied to describe the plate bending problem. The expressions for the bending moment, shear force and normal force are obtained by integration through the FGM plate and magnetoelectric layer for the corresponding constitutive equations. Then, the original three-dimensional (3D) thick-plate problem is reduced to a two-dimensional (2D) problem. Nodal points are randomly distributed over the mean surface of the considered plate. Each node is the center of a circle surrounding the node. The weak-form on small subdomains with a Heaviside step function as the test function is applied to derive local integral equations. After performing the spatial MLS approximation, a system of ordinary differential equations of the second order for certain nodal unknowns is obtained. The derived ordinary differential equations are solved by the Houbolt finite-difference scheme. Pure mechanical loads or electromagnetic potentials are prescribed on the top of the layered plate. Both stationary and transient dynamic loads are analyzed.

1. Introduction

A number of materials have been used for active control of smart structures. Piezoelectric materials, magnetostrictive materials, shape memory alloys, and electro-rheological fluids have all been integrated with structures to make smart structures. Among them, piezoelectric, electrostrictive and magnetostrictive materials have the capability to serve as both sensors and actuators. Distributed piezoelectric sensors and actuators are frequently used for active vibration control of various elastic structures [1–3]. It requires finding the optimum number and placement of actuators and sensors for a given plate [4]. Batra *et al* [5] analyzed a similar problem with fixed PZT layers on the top and bottom of the plate. A rich literature survey is available on the shape control of structures, especially through the application of piezoelectric materials [6]. The PZT actuators are usually poled in the plate thickness direction. If an electric field is applied in the plate thickness direction, the actuator lateral dimensions are charged and strains are induced in the host plate. Mechanical models for studying the interaction of piezoelectric patches fixed to a beam have been developed by Crawley and de Luis [7], and Im and Atluri [8]. Later, the fully coupled electromechanical theories have been applied. Thornburgh and Chattopadhyay [9] used a higher-order laminated plate theory to study deformations of smart structures.

An ideal actuator, for distributed embedded application, should have high energy density, negligible weight, and point excitation with a wide frequency bandwidth. Terfenol-D, a magnetostrictive material, has the characteristics of being able to produce large strains in response to a magnetic field [10]. Krishna Murty *et al* [11] proposed magnetostrictive actuators that take advantage of the ease with which the actuators can be embedded, and the use of the remote excitation capability of magnetostrictive particles as new actuators for smart structures. Friedmann *et al* [12] used the magnetostrictive material Terfenol-D in high-speed helicopter rotors and studied the vibration reduction characteristics. Recently, magnetoelectroelastic (MEE) materials have found many applications as sensors and actuators for the purpose of monitoring and controlling the response of structures, respectively. The MEE layers are frequently embedded into laminated composite plates to control the shape of plates. The magnetoelectric forces give rise to strains that can reduce the effects of the applied mechanical load. Thus structures can be designed using less material and hence less weight. Pan [13] and Pan and Heyliger [14] presented the analytical solution for the analysis of simply supported MEE laminated

 © 2013 IOP Publishing Ltd Printed in the UK & the USA

rectangular plates, regarding static and free vibration. Wang and Shen [15] obtained the general solution of the 3D problem in transversely isotropic MEE media. Chen *et al* [16] established a micromechanical model for the evaluation of the effective properties in layered composites with piezoelectric and piezomagnetic phases. Zheng *et al* [17] presented a new class of active and passive magnetic constrained layer damping treatment for controlling the vibration of three-layer clamped–clamped beams. Lage *et al* [18] applied the layerwise partial mixed finite element analysis for MEE plates.

A special class of composite materials known collectively as functionally graded materials or FGMs, first developed in the late 1980s, is characterized by the smooth and continuous change of mechanical properties with Cartesian coordinates (Miyamoto *et al* [19]). As far as the authors are aware, very limited works can be found in the literature for the active control of FGM structures. There are some papers where only piezoelectric elements are utilized for active control of the FGM plates. Liew *et al* [20] have developed a finite element formulation based on the first-order shear deformation theory for static and dynamic piezothermoelastic analysis and active control of FGM plates subjected to a temperature gradient using integrated piezoelectric sensor/actuator layers. No paper has been published to date for active control of FGM plates by MEE elements.

The solution of a general boundary or initial boundary value problems for laminated MEE plates requires advanced numerical methods due to the high mathematical complexity. Besides the well established FEM, the meshless method provides an efficient and popular alternative to the FEM. The elimination of shear locking in thin-walled structures by FEM is difficult and the developed techniques are less accurate. Focusing only on nodes or points instead of elements used in the conventional FEM, meshless approaches have certain advantages. The moving least-square (MLS) approximation ensures C^1 continuity which satisfies the Kirchhoff hypotheses. The continuity of the MLS approximation is given by the minimum between the continuity of the basis functions and that of the weight function. So continuity can be tuned to a desired degree. The results showed excellent convergence; however, the formulation has not been applied to shear deformable laminated MEE plate problems to date. The meshless methods are very appropriate for modeling nonlinear plate problems [21]. One of the most rapidly developed meshfree methods is the meshless local Petrov–Galerkin (MLPG) method. The MLPG method has attracted much attention during the past decade [22–27] for many problems in continuum mechanics.

In the present paper we will present for the first time a meshless method based on the local Petrov–Galerkin weak-form to solve dynamic problems for the FGM plate with MEE layer used as a sensor or actuator. The bending moment and shear force expressions are obtained by integration through the laminated plate for the considered constitutive equations in the FGM plate and MEE layer. It should be pointed out that, for FGM, the variation of the induced field quantities in the thickness direction would be more complicated [28] and one should be cautious when introducing FGM into the system. The Reissner–Mindlin governing equations of motion are subsequently solved for an elastodynamic plate bending problem. It allows one to reduce the original 3D thick-plate problem to a 2D problem. Nodal points are randomly distributed over the mean surface of the considered plate. Each node is the center of a circle surrounding this node. A similar approach has been successfully applied to Reissner–Mindlin plates and shells under dynamic load [29, 30]. Long and Atluri [31] applied the meshless local Petrov–Galerkin method to solve the bending problem of a thin plate. Soric *et al* [32] have performed a 3D analysis of thick plates, where a plate is divided by small cylindrical subdomains for which the MLPG is applied. Homogeneous material properties of plates are considered in previous papers.

The weak-form on small subdomains with a Heaviside step function as the test functions is applied to derive local integral equations. Applying the Gauss divergence theorem to the weak-form, the local boundary-domain integral equations are derived. After performing the spatial MLS approximation, a system of ordinary differential equations for certain nodal unknowns is obtained. Then, the system of second-order ordinary differential equations resulting from the equations of motion is solved by the Houbolt finite-difference scheme [33] as a time-stepping method. Numerical examples are presented and discussed to show the accuracy and efficiency of the present method.

2. Local integral equations for laminated plate theory

A laminate plate contains the FGM plate and a MEE layer bonded on the top of the elastic plate. Consider a plate of total thickness h composed of two layers with the mean surface occupying the domain Ω in the plane (x_1, x_2). The thickness of the FGM plate is considered to be h_1 and the MEE layer to be $h_2 = z_3 - z_2$. The $x_3 \equiv z$ axis is perpendicular to the mid-plane (figure 1) with the origin at the bottom of the plate.

The spatial displacement field has the following form [34]

$$\begin{aligned} u_1(\mathbf{x}, x_3, \tau) &= u_0 + (z - z_{011}) w_1(\mathbf{x}, \tau), \\ u_2(\mathbf{x}, x_3, \tau) &= v_0 + (z - z_{022}) w_2(\mathbf{x}, \tau), \\ u_3(\mathbf{x}, \tau) &= w_3(\mathbf{x}, \tau), \end{aligned} \tag{1}$$

where z_{011} and z_{022} indicate the position of the neutral plane in the x_1- and x_2-direction, respectively. In-plane displacements are denoted by u_0 and v_0, rotations around x_1- and x_2-axes are denoted by w_1 and w_2, respectively, and w_3 is the out-of-plane deflection. The linear strains are given by

$$\begin{aligned} &\varepsilon_{11}(\mathbf{x}, x_3, \tau) = u_{0,1}(\mathbf{x}, \tau) + (z - z_{011}) w_{1,1}(\mathbf{x}, \tau), \\ &\varepsilon_{22}(\mathbf{x}, x_3, \tau) = v_{0,2}(\mathbf{x}, \tau) + (z - z_{022}) w_{2,2}(\mathbf{x}, \tau), \\ &\varepsilon_{12}(\mathbf{x}, x_3, \tau) = [u_{0,2}(\mathbf{x}, \tau) + v_{0,1}(\mathbf{x}, \tau)]/2 \\ &\qquad + [(z - z_{011}) w_{1,2}(\mathbf{x}, \tau) + (z - z_{022}) w_{2,1}(\mathbf{x}, \tau)]/2, \\ &\varepsilon_{13}(\mathbf{x}, \tau) = [w_1(\mathbf{x}, \tau) + w_{3,1}(\mathbf{x}, \tau)]/2, \\ &\varepsilon_{23}(\mathbf{x}, \tau) = [w_2(\mathbf{x}, \tau) + w_{3,2}(\mathbf{x}, \tau)]/2. \end{aligned} \tag{2}$$

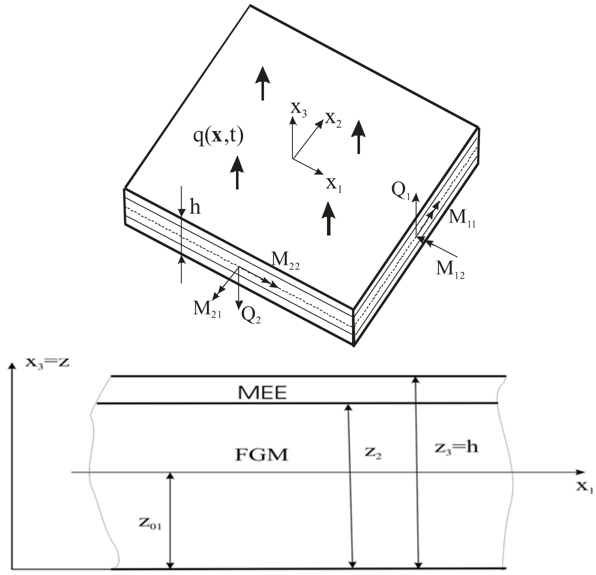

Figure 1. Sign convention of bending moments, forces and layer numbering for a laminate plate.

The FGM plate with pure elastic properties can be considered as a special MEE material with vanishing piezoelectric and piezomagnetic coefficients. Then, the FGM plate with a MEE layer can be analyzed generally as a laminated plate with corresponding constitutive equations. The variation of material parameters with Cartesian coordinates has to be considered there. The constitutive equations for the stress tensor, the electrical displacement and the magnetic induction are given by Nan [35]

$$\sigma_{ij}(\mathbf{x}, x_3, \tau) = c_{ijkl}(\mathbf{x})\varepsilon_{kl}(\mathbf{x}, x_3, \tau) - e_{kij}(\mathbf{x})E_k(\mathbf{x}, x_3, \tau) - d_{kij}(\mathbf{x})H_k(\mathbf{x}, x_3, \tau), \tag{3}$$

$$D_j(\mathbf{x}, x_3, \tau) = e_{jkl}(\mathbf{x})\varepsilon_{kl}(\mathbf{x}, x_3, \tau) + h_{jk}(\mathbf{x})E_k(\mathbf{x}, x_3, \tau) + \alpha_{jk}(\mathbf{x})H_k(\mathbf{x}, x_3, \tau), \tag{4}$$

$$B_j(\mathbf{x}, x_3, \tau) = d_{jkl}(\mathbf{x})\varepsilon_{kl}(\mathbf{x}, x_3, \tau) + \alpha_{kj}(\mathbf{x})E_k(\mathbf{x}, x_3, \tau) + \gamma_{jk}(\mathbf{x})H_k(\mathbf{x}, x_3, \tau), \tag{5}$$

where $\{\varepsilon_{ij}, E_\mathrm{i}, H_\mathrm{i}\}$ is the set of secondary field quantities (strains, intensity of electric field, intensity of magnetic field) which are expressed in terms of the gradients of the primary fields such as the elastic displacement vector, potential of electric field, and potential of magnetic field $\{u_\mathrm{i}, \psi, \mu\}$, respectively. Finally, the elastic stress tensor, electric displacement, and magnetic induction vectors $\{\sigma_{ij}, D_\mathrm{i}, B_\mathrm{i}\}$ form the set of fields conjugated with the secondary fields $\{\varepsilon_{ij}, E_\mathrm{i}, H_\mathrm{i}\}$. The constitutive equations correlate these two last sets of fields in continuum media including the multifield interactions.

The plate thickness is assumed to be small as compared to its in-plane dimensions. The normal stress σ_{33} is negligible in comparison with other normal stresses. In the case of some crystal symmetries, one can formulate also the plane-deformation problems [36]. For the poling direction along the positive x_3-axis, equations (3)–(5) are reduced to the following matrix forms

$$\begin{bmatrix}\sigma_{11}\\ \sigma_{22}\\ \sigma_{12}\\ \sigma_{13}\\ \sigma_{23}\end{bmatrix} = \begin{bmatrix} c_{11} & c_{12} & 0 & 0 & 0\\ c_{12} & c_{22} & 0 & 0 & 0\\ 0 & 0 & c_{66} & 0 & 0\\ 0 & 0 & 0 & c_{55} & 0\\ 0 & 0 & 0 & 0 & c_{44}\end{bmatrix}\begin{bmatrix}\varepsilon_{11}\\ \varepsilon_{22}\\ 2\varepsilon_{12}\\ 2\varepsilon_{13}\\ 2\varepsilon_{23}\end{bmatrix} - \begin{bmatrix} 0 & 0 & e_{31}\\ 0 & 0 & e_{32}\\ 0 & 0 & 0\\ e_{15} & 0 & 0\\ 0 & e_{15} & 0\end{bmatrix}\begin{bmatrix}E_1\\ E_2\\ E_3\end{bmatrix} - \begin{bmatrix} 0 & 0 & d_{31}\\ 0 & 0 & d_{32}\\ 0 & 0 & 0\\ d_{15} & 0 & 0\\ 0 & d_{15} & 0\end{bmatrix}$$
$$\times \begin{bmatrix}H_1\\ H_2\\ H_3\end{bmatrix} \equiv \mathbf{C}\begin{bmatrix}\varepsilon_{11}\\ \varepsilon_{22}\\ 2\varepsilon_{12}\\ 2\varepsilon_{13}\\ 2\varepsilon_{23}\end{bmatrix} - \mathbf{L}\begin{bmatrix}E_1\\ E_2\\ E_3\end{bmatrix} - \mathbf{K}\begin{bmatrix}H_1\\ H_2\\ H_3\end{bmatrix}, \tag{6}$$

$$\begin{bmatrix}D_1\\ D_2\\ D_3\end{bmatrix} = \begin{bmatrix} 0 & 0 & 0 & e_{15} & 0\\ 0 & 0 & 0 & 0 & e_{15}\\ e_{31} & e_{32} & 0 & 0 & 0\end{bmatrix}\begin{bmatrix}\varepsilon_{11}\\ \varepsilon_{22}\\ 2\varepsilon_{12}\\ 2\varepsilon_{13}\\ 2\varepsilon_{23}\end{bmatrix} + \begin{bmatrix} h_{11} & 0 & 0\\ 0 & h_{22} & 0\\ 0 & 0 & h_{33}\end{bmatrix}\begin{bmatrix}E_1\\ E_2\\ E_3\end{bmatrix} + \begin{bmatrix} \alpha_{11} & 0 & 0\\ 0 & \alpha_{22} & 0\\ 0 & 0 & \alpha_{33}\end{bmatrix}$$
$$\times \begin{bmatrix}H_1\\ H_2\\ H_3\end{bmatrix} \equiv \mathbf{G}\begin{bmatrix}\varepsilon_{11}\\ \varepsilon_{22}\\ 2\varepsilon_{12}\\ 2\varepsilon_{13}\\ 2\varepsilon_{23}\end{bmatrix} + \mathbf{H}\begin{bmatrix}E_1\\ E_2\\ E_3\end{bmatrix} + \mathbf{A}\begin{bmatrix}H_1\\ H_2\\ H_3\end{bmatrix}, \tag{7}$$

$$\begin{bmatrix}B_1\\ B_2\\ B_3\end{bmatrix} = \begin{bmatrix} 0 & 0 & 0 & d_{15} & 0\\ 0 & 0 & 0 & 0 & d_{15}\\ d_{31} & d_{32} & 0 & 0 & 0\end{bmatrix}\begin{bmatrix}\varepsilon_{11}\\ \varepsilon_{22}\\ 2\varepsilon_{12}\\ 2\varepsilon_{13}\\ 2\varepsilon_{23}\end{bmatrix} + \begin{bmatrix} \alpha_{11} & 0 & 0\\ 0 & \alpha_{22} & 0\\ 0 & 0 & \alpha_{33}\end{bmatrix}\begin{bmatrix}E_1\\ E_2\\ E_3\end{bmatrix} + \begin{bmatrix} \gamma_{11} & 0 & 0\\ 0 & \gamma_{22} & 0\\ 0 & 0 & \gamma_{33}\end{bmatrix}$$
$$\times \begin{bmatrix}H_1\\ H_2\\ H_3\end{bmatrix} \equiv \mathbf{R}\begin{bmatrix}\varepsilon_{11}\\ \varepsilon_{22}\\ 2\varepsilon_{12}\\ 2\varepsilon_{13}\\ 2\varepsilon_{23}\end{bmatrix} + \mathbf{A}\begin{bmatrix}E_1\\ E_2\\ E_3\end{bmatrix} + \mathbf{M}\begin{bmatrix}H_1\\ H_2\\ H_3\end{bmatrix}. \tag{8}$$

Maxwell's vector equations in the quasi-static approximation are satisfied if the electric vector and magnetic intensity are expressed as gradients of the scalar electric and magnetic potentials $\psi(\mathbf{x}, \tau)$ and $\mu(\mathbf{x}, \tau)$, respectively [36],

$$E_j = -\psi_{,j}, \tag{9}$$

$$H_j = -\mu_{,j}. \tag{10}$$

Since the MEE layer is thin, the in-plane electric and magnetic fields can be ignored, i.e., $E_1 = E_2 = 0$ and $H_1 = H_2 = 0$ [37]. It is reasonable to assume that $\left(|D_{1,1}|, |D_{2,2}|\right) \ll |D_{3,3}|$ [2] and $(|B_{1,1}|, |B_{2,2}|) \ll |B_{3,3}|$. Then, the Maxwell equations are reduced to:

$$D_{3,3} = 0. \tag{11}$$

$$B_{3,3} = 0. \tag{12}$$

The electric and magnetic potentials in the elastic FGM plate vanish. In the MEE layer both potentials are assumed to be varying quadratically in the z direction:

$$\psi(\mathbf{x}, z, \tau) = \psi_1(\mathbf{x}, \tau)\frac{z - z_2}{h_2} + \psi_2(\mathbf{x}, \tau)(z - z_2)^2, \tag{13}$$

$$\mu(\mathbf{x}, z, \tau) = \mu_1(\mathbf{x}, \tau)\frac{z - z_2}{h_2} + \mu_2(\mathbf{x}, \tau)(z - z_2)^2. \tag{14}$$

Substituting potentials (13) and (14) into the electrical displacement and magnetic induction expressions (7) and (8) one obtains

$$\begin{aligned} D_3(\mathbf{x}, z, \tau) = {} & e_{31}\left[u_{0,1}(\mathbf{x}, \tau) + w_{1,1}(\mathbf{x}, \tau)(z - z_{011})\right] \\ & + e_{32}\left[v_{0,2}(\mathbf{x}, \tau) + w_{2,2}(\mathbf{x}, \tau)(z - z_{022})\right] \\ & - h_{33}\frac{\psi_1(\mathbf{x}, \tau)}{h} - 2h_{33}\psi_2(\mathbf{x}, \tau)(z - z_2) \\ & - \alpha_{33}\frac{\mu_1(\mathbf{x}, \tau)}{h} - 2\alpha_{33}\mu_2(\mathbf{x}, \tau)\,(z - z_2)\,, \end{aligned} \tag{15}$$

$$\begin{aligned} B_3(\mathbf{x}, z, \tau) = {} & d_{31}\left[u_{0,1}(\mathbf{x}, \tau) + w_{1,1}(\mathbf{x}, \tau)(z - z_{011})\right] \\ & + d_{32}\left[v_{0,2}(\mathbf{x}, \tau) + w_{2,2}(\mathbf{x}, \tau)(z - z_{022})\right] \\ & - \alpha_{33}\frac{\psi_1(\mathbf{x}, \tau)}{h} - 2\alpha_{33}\psi_2(\mathbf{x}, \tau)(z - z_2) \\ & - \gamma_{33}\frac{\mu_1(\mathbf{x}, \tau)}{h} - 2\gamma_{33}\mu_2(\mathbf{x}, \tau)(z - z_2). \end{aligned} \tag{16}$$

Both expressions have to satisfy the Maxwell equations (11) and (12). Then, one gets the expressions for ψ_2 and μ_2

$$\psi_2(\mathbf{x}, \tau) = \frac{(\alpha_{33}d_{31} - e_{31}\gamma_{33})\,w_{1,1}(\mathbf{x}, \tau) + (d_{32}\alpha_{33} - e_{32}\gamma_{33})\,w_{2,2}(\mathbf{x}, \tau)}{2\,(\alpha_{33}\alpha_{33} - \gamma_{33}h_{33})}, \tag{17}$$

$$\mu_2(\mathbf{x}, \tau) = \frac{(e_{31}\alpha_{33} - d_{31}h_{33})\,w_{1,1}(\mathbf{x}, \tau) + (e_{32}\alpha_{33} - d_{32}h_{33})\,w_{2,2}(\mathbf{x}, \tau)}{2\,(\alpha_{33}\alpha_{33} - \gamma_{33}h_{33})}. \tag{18}$$

The position of the neutral planes in a pure bending case (vanishing electric and magnetic fields) is obtained from the condition (no summation is assumed through α)

$$\int_0^h \sigma_{\alpha\alpha}(\mathbf{x}, z, \tau)\,\mathrm{d}z = 0, \qquad \text{for } \alpha = 1, 2. \tag{19}$$

Consider a two-layered composite with layer thicknesses h_1 and h_2, and the corresponding material parameters $c^{(1)}_{\alpha\beta}$ and $c^{(2)}_{\alpha\beta}$. In the first FGM layer, one can assume a polynomial variation of material parameters as

$$c^{(1)}_{\alpha\beta} = c^{(1)}_{\alpha\beta b} + \left(c^{(1)}_{\alpha\beta t} - c^{(1)}_{\alpha\beta b}\right)\left(\frac{z}{h_1}\right)^n \tag{20}$$

with $c^{(1)}_{\alpha\beta b}$ and $c^{(1)}_{\alpha\beta t}$ corresponding to material parameters on the bottom and top surfaces of the plate and n being the exponent. We then get the position of the neutral plane for individual deformations

$$z_{o\alpha\alpha} = \frac{c^{(1)}_{\alpha\alpha b}h_1^2 - (c^{(1)}_{\alpha\alpha t} - c^{(1)}_{\alpha\alpha b})h_1^2\frac{2}{n+2} + c^{(2)}_{\alpha\alpha}(h_2^2 + 2h_1h_2)}{2[c^{(2)}_{\alpha\alpha}h_2 + c^{(1)}_{\alpha\alpha b}h_1 - (c^{(1)}_{\alpha\alpha t} - c^{(1)}_{\alpha\alpha b})\frac{h_1}{n+1}]}. \tag{21}$$

Generally we have two neutral planes if the material properties in directions 1 and 2 are different. For the bending moment M_{12} we should define a neutral plane too. We can generalize formula (21) to replace $c^{(i)}_{\alpha\alpha}$ by $c^{(i)}_{66}$ to get z_{012}.

Despite the stress discontinuities, one can define integral quantities such as the bending moments $M_{\alpha\beta}$, shear forces Q_α and normal stresses $N_{\alpha\beta}$ as

$$\begin{aligned} \begin{bmatrix} M_{11} \\ M_{22} \\ M_{12} \end{bmatrix} &= \int_0^h \begin{bmatrix} \sigma_{11} \\ \sigma_{22} \\ \sigma_{12} \end{bmatrix} (z - z_{0\alpha\beta})\,\mathrm{d}z \\ &= \sum_{k=1}^{N} \int_{z_k}^{z_{k+1}} \begin{bmatrix} \sigma_{11} \\ \sigma_{22} \\ \sigma_{12} \end{bmatrix}^{(k)} (z - z_{0\alpha\beta})\,\mathrm{d}z \\ \begin{bmatrix} Q_1 \\ Q_2 \end{bmatrix} &= \kappa \int_0^h \begin{bmatrix} \sigma_{13} \\ \sigma_{23} \end{bmatrix} \mathrm{d}z = \kappa \sum_{k=1}^{N} \int_{z_k}^{z_{k+1}} \begin{bmatrix} \sigma_{13} \\ \sigma_{23} \end{bmatrix}^{(k)} \mathrm{d}z, \\ \begin{bmatrix} N_{11} \\ N_{22} \\ N_{12} \end{bmatrix} &= \int_0^h \begin{bmatrix} \sigma_{11} \\ \sigma_{22} \\ \sigma_{12} \end{bmatrix} \mathrm{d}z = \sum_{k=1}^{N} \int_{z_k}^{z_{k+1}} \begin{bmatrix} \sigma_{11} \\ \sigma_{22} \\ \sigma_{12} \end{bmatrix}^{(k)} \mathrm{d}z, \end{aligned} \tag{22}$$

where $\kappa = 5/6$, as in the Reissner plate theory.

Substituting equations (2) and (6) into the formulas for the moment and forces (22) and considering the FGM properties (20), we obtain the expression of the bending moments $M_{\alpha\beta}$, shear forces Q_α and normal stresses $N_{\alpha\beta}$ for $\alpha, \beta = 1, 2$, in terms of rotations, lateral displacements and electric potential of the layered plate. Expressions are given in appendix A.

By ignoring the coupling effect from inertia forces between in-plane and bending cases, one has the governing equations in the following form [38]:

$$M_{\alpha\beta,\beta}(\mathbf{x}, \tau) - Q_\alpha(\mathbf{x}, \tau) = I_{M\alpha}\ddot{w}_\alpha(\mathbf{x}, \tau), \tag{23}$$

$$Q_{\alpha,\alpha}(\mathbf{x}, \tau) + q(\mathbf{x}, \tau) = I_Q\ddot{w}_3(\mathbf{x}, \tau), \tag{24}$$

$$N_{\alpha\beta,\beta}(\mathbf{x}, \tau) + q_\alpha(\mathbf{x}, \tau) = I_Q\ddot{u}_{\alpha 0}(\mathbf{x}, \tau), \qquad \mathbf{x} \in \Omega, \tag{25}$$

where

$$\begin{aligned} I_{M\alpha} &= \int_0^h (z - z_{0\alpha\alpha})^2 \rho(z)\,\mathrm{d}z \\ &= \sum_{k=1}^{2} \int_{z_k}^{z_{k+1}} \rho^{(k)} (z - z_{0\alpha\alpha})^2\,\mathrm{d}z \\ &= \sum_{k=1}^{N} \rho^{(k)} [\tfrac{1}{3}(z_{k+1}^3 - z_k^3) \\ &\quad - z_{0\alpha\alpha}(z_{k+1}^2 - z_k^2) + z_{0\alpha\alpha}^2 (z_{k+1} - z_k)], \end{aligned}$$

$$I_Q = \int_0^h \rho(z)\,\mathrm{d}z = \sum_{k=1}^{2} \int_{z_k}^{z_{k+1}} \rho^{(k)}\,\mathrm{d}z = \sum_{k=1}^{N} \rho^{(k)}\,(z_{k+1} - z_k)$$

are global inertial characteristics of the laminate plate. If the mass density is constant throughout the plate thickness, we obtain

$$I_M = \frac{\rho h^3}{12}, \qquad I_Q = \rho h.$$

Throughout the analysis, the Greek indices vary from 1 to 2, and the dots over a quantity indicate differentiations with respect to time τ. A transversal load is denoted by $q(\mathbf{x}, \tau)$, and $q_\alpha(\mathbf{x}, \tau)$ represents the in-plane load.

The governing equations (23)–(25) contain 5 equations for 7 unknowns $(w_1, w_2, w_3, u_0, v_0, \psi_1, \mu_1)$. Therefore, we need two additional equations for the unknown ψ_1 and μ_1. There are two possibilities to prescribe the electromagnetic conditions:

(a) The layered plate is under a mechanical load and the electromagnetic potentials are induced on the top surface of the plate. The MEE layer is then used as a sensor. Thus, the electric displacement D_3 and magnetic induction B_3 given by equations (15) and (16) vanish on the top surface

$$\begin{aligned} & e_{31}[u_{0,1}(\mathbf{x}, \tau) + w_{1,1}(\mathbf{x}, \tau)(h - z_{011})] \\ &\quad + e_{32}[v_{0,2}(\mathbf{x}, \tau) + w_{2,2}(\mathbf{x}, \tau)(h - z_{022})] \\ &\quad - h_{33}\frac{\psi_1(\mathbf{x}, \tau)}{h_2} - 2h_{33}\psi_2(\mathbf{x}, \tau) h_2 - \alpha_{33}\frac{\mu_1(\mathbf{x}, \tau)}{h_2} \\ &\quad - 2\alpha_{33}\mu_2(\mathbf{x}, \tau) h_2 = 0, \end{aligned} \tag{26}$$

$$\begin{aligned} & d_{31}[u_{0,1}(\mathbf{x}, \tau) + w_{1,1}(\mathbf{x}, \tau)(h - z_{011})] \\ &\quad + d_{32}[v_{0,2}(\mathbf{x}, \tau) + w_{2,2}(\mathbf{x}, \tau)(h - z_{022})] \\ &\quad - \alpha_{33}\frac{\psi_1(\mathbf{x}, \tau)}{h_2} - 2\alpha_{33}\psi_2(\mathbf{x}, \tau) h_2 - \gamma_{33}\frac{\mu_1(\mathbf{x}, \tau)}{h_2} \\ &\quad - 2\gamma_{33}\mu_2(\mathbf{x}, \tau) h_2 = 0. \end{aligned} \tag{27}$$

The governing equations (23)–(25) with two additional equations (26) and (27) give a unique formulation for the solution of the layered plate under a mechanical load.

(b) The plate under prescribed electromagnetic potentials is deformed and is now used as an actuator. Finite values of potentials, $\tilde{\psi}$ and $\tilde{\mu}$, are prescribed on the top surface and vanishing values on the bottom,

$$\psi(\mathbf{x}, h, \tau) = \tilde{\psi} = \psi_1(\mathbf{x}, \tau) + \psi_2(\mathbf{x}, \tau) h_2^2, \tag{28}$$

$$\mu(\mathbf{x}, h, \tau) = \tilde{\mu} = \mu_1(\mathbf{x}, \tau) + \mu_2(\mathbf{x}, \tau) h_2^2. \tag{29}$$

Substituting equations (17) and (18) into (28) and (29), respectively, we obtain expressions for ψ_1 and μ_1

$$\begin{aligned} \psi_1(\mathbf{x}, \tau) &= \tilde{\psi} \\ &- \frac{(\alpha_{33}d_{31} - e_{31}\gamma_{33})\, w_{1,1}(\mathbf{x}, \tau) + (d_{32}\alpha_{33} - e_{32}\gamma_{33})\, w_{2,2}(\mathbf{x}, \tau)}{2\,(\alpha_{33}\alpha_{33} - \gamma_{33}h_{33})} h_2^2, \end{aligned} \tag{30}$$

$$\begin{aligned} \mu_1(\mathbf{x}, \tau) &= \tilde{\mu} \\ &- \frac{(e_{31}\alpha_{33} - d_{31}h_{33})\, w_{1,1}(\mathbf{x}, \tau) + (e_{32}\alpha_{33} - d_{32}h_{33})\, w_{2,2}(\mathbf{x}, \tau)}{2\,(\alpha_{33}\alpha_{33} - \gamma_{33}h_{33})} h_2^2. \end{aligned} \tag{31}$$

In this case the unknowns are reduced to three mechanical quantities, since electromagnetic quantities with quadratic approximation along the thickness of MEE layer are expressed through mechanical ones.

The MLPG method constructs the weak-form over local subdomains such as Ω_s, which is a small region taken for each node inside the global domain [24]. The local subdomains could be of any geometrical shape and size. In the current paper, the local subdomains are taken to be of circular shape. The local weak-form of the governing equations (23)–(25) for $\mathbf{x}^i \in \Omega_s^i$ can be written as

$$\begin{aligned} & \int_{\Omega_s^i} \left[M_{\alpha\beta,\beta}(\mathbf{x}, \tau) - Q_\alpha(\mathbf{x}, \tau) - I_{M\alpha}\ddot{w}_\alpha(\mathbf{x}, \tau) \right] \\ &\quad \times w_{\alpha\gamma}^*(\mathbf{x})\,\mathrm{d}\Omega = 0, \end{aligned} \tag{32}$$

$$\begin{aligned} & \int_{\Omega_s^i} \left[Q_{\alpha,\alpha}(\mathbf{x}, \tau) + q(\mathbf{x}, \tau) - I_Q\ddot{w}_3(\mathbf{x}, \tau) \right] \\ &\quad \times w^*(\mathbf{x})\,\mathrm{d}\Omega = 0, \end{aligned} \tag{33}$$

$$\begin{aligned} & \int_{\Omega_s^i} \left[N_{\alpha\beta,\chi}(\mathbf{x}, \tau) + q_\alpha(\mathbf{x}, \tau) - I_Q\ddot{u}_{\alpha 0}(\mathbf{x}, \tau) \right] \\ &\quad \times w_{\alpha\gamma}^*(\mathbf{x})\,\mathrm{d}\Omega = 0, \end{aligned} \tag{34}$$

where $w_{\alpha\beta}^*(\mathbf{x})$ and $w^*(\mathbf{x})$ are weight or test functions.

Applying the Gauss divergence theorem to equations (32)–(34) one obtains

$$\begin{aligned} & \int_{\partial\Omega_s^i} M_\alpha(\mathbf{x}, \tau) w_{\alpha\gamma}^*(\mathbf{x})\,\mathrm{d}\Gamma - \int_{\Omega_s^i} M_{\alpha\beta}(\mathbf{x}, \tau) w_{\alpha\gamma,\beta}^*(\mathbf{x})\,\mathrm{d}\Omega \\ &\quad - \int_{\Omega_s^i} Q_\alpha(\mathbf{x}, \tau) w_{\alpha\gamma}^*(\mathbf{x})\,\mathrm{d}\Omega \\ &\quad - \int_{\Omega_s^i} I_{M\alpha}\ddot{w}_\alpha(\mathbf{x}, \tau) w_{\alpha\gamma}^*(\mathbf{x})\,\mathrm{d}\Omega = 0, \end{aligned} \tag{35}$$

$$\begin{aligned} & \int_{\partial\Omega_s^i} Q_\alpha(\mathbf{x}, \tau) n_\alpha(\mathbf{x}) w^*(\mathbf{x})\mathrm{d}\Gamma - \int_{\Omega_s^i} Q_\alpha(\mathbf{x}, \tau) w_{,\alpha}^*(\mathbf{x})\,\mathrm{d}\Omega \\ &\quad - \int_{\Omega_s^i} I_Q\ddot{w}_3(\mathbf{x}, \tau) w^*(\mathbf{x})\,\mathrm{d}\Omega \\ &\quad + \int_{\Omega_s^i} q(\mathbf{x}, \tau) w^*(\mathbf{x})\,\mathrm{d}\Omega = 0, \end{aligned} \tag{36}$$

$$\begin{aligned} & \int_{\partial\Omega_s^i} N_\alpha(\mathbf{x}, \tau) w_{\alpha\gamma}^*(\mathbf{x})\,\mathrm{d}\Gamma - \int_{\Omega_s^i} N_{\alpha\beta}(\mathbf{x}, \tau) w_{\alpha\gamma,\beta}^*(\mathbf{x})\,\mathrm{d}\Omega \\ &\quad + \int_{\Omega_s^i} q_\alpha(\mathbf{x}, \tau) w_{\alpha\gamma}^*(\mathbf{x})\,\mathrm{d}\Omega \\ &\quad - \int_{\Omega_s^i} I_Q\ddot{u}_{\alpha 0}(\mathbf{x}, \tau) w_{\alpha\gamma}^*(\mathbf{x})\,\mathrm{d}\Omega = 0, \end{aligned} \tag{37}$$

where $\partial\Omega_s^i$ is the boundary of the local subdomain and

$$M_\alpha(\mathbf{x}, \tau) = M_{\alpha\beta}(\mathbf{x}, \tau) n_\beta(\mathbf{x})$$

and

$$N_\alpha(\mathbf{x},\tau) = N_{\alpha\beta}(\mathbf{x},\tau)n_\beta(\mathbf{x})$$

are the normal bending moment and traction vector, respectively, and n_α is the unit outward normal vector to the boundary $\partial\Omega_s^i$. The local weak-forms (35)–(37) are the starting point for deriving local boundary integral equations on the basis of the appropriate test functions. Unit step functions are chosen for the test functions $w^*_{\alpha\beta}(\mathbf{x})$ and $w^*(\mathbf{x})$ in each subdomain

$$w^*_{\alpha\gamma}(\mathbf{x}) = \begin{cases} \delta_{\alpha\gamma} & \text{at } \mathbf{x} \in (\Omega_s \cup \partial\Omega_s) \\ 0 & \text{at } \mathbf{x} \notin (\Omega_s \cup \partial\Omega_s), \end{cases}$$
$$w^*(\mathbf{x}) = \begin{cases} 1 & \text{at } \mathbf{x} \in (\Omega_s \cup \partial\Omega_s) \\ 0 & \text{at } \mathbf{x} \notin (\Omega_s \cup \partial\Omega_s). \end{cases} \tag{38}$$

Then, the local weak-forms (35)–(37) are transformed into the following local integral equations (LIEs)

$$\int_{\partial\Omega_s^i} M_\alpha(\mathbf{x},\tau)\,d\Gamma - \int_{\Omega_s^i} Q_\alpha(\mathbf{x},\tau)\,d\Omega - \int_{\Omega_s^i} I_{M\alpha}\ddot{w}_\alpha(\mathbf{x},\tau)\,d\Omega = 0, \tag{39}$$

$$\int_{\partial\Omega_s^i} Q_\alpha(\mathbf{x},\tau)n_\alpha(\mathbf{x})\,d\Gamma - \int_{\Omega_s^i} I_Q\ddot{w}_3(\mathbf{x},\tau)\,d\Omega + \int_{\Omega_s^i} q(\mathbf{x},\tau)\,d\Omega = 0. \tag{40}$$

$$\int_{\partial\Omega_s^i} N_\alpha(\mathbf{x},\tau)\,d\Gamma + \int_{\Omega_s^i} q_\alpha(\mathbf{x},\tau)\,d\Omega - \int_{\Omega_s^i} I_Q\ddot{u}_{\alpha 0}(\mathbf{x},\tau)\,d\Omega = 0. \tag{41}$$

In the above local integral equations, the trial functions $w_\alpha(\mathbf{x},\tau)$ related to rotations, $w_3(\mathbf{x},\tau)$ related to transversal displacements, and $u_{\alpha 0}(\mathbf{x},\tau)$ the in-plane displacements, are chosen as the moving least-squares (MLS) approximations over a number of nodes randomly spread within the influence domain.

3. Numerical solution

In general, a meshless method uses a local interpolation to represent the trial function with the values (or the fictitious values) of the unknown variable at some randomly located nodes. The moving least-squares (MLS) approximation [39, 40] used in the present analysis may be considered as one of such schemes. According to the MLS method [24], the approximation of the field variable $u \in \{w_1, w_2, w_3, u_0, v_0, \psi_1, \mu_1\}$ can be given as

$$u^h(\mathbf{x},\tau) = \mathbf{\Phi}^{\mathrm{T}}(\mathbf{x})\cdot\hat{\mathbf{u}} = \sum_{a=1}^{n} \phi^a(\mathbf{x})\hat{u}^a(\tau), \tag{42}$$

where the nodal values $\hat{u}^a(\tau)$ are fictitious parameters for the approximated field variable and $\phi^a(\mathbf{x})$ is the shape function associated with the node a. The number of nodes n used for the approximation is determined by the weight function $w^a(\mathbf{x})$. A 4th-order spline-type weight function is applied in the present work.

The directional derivatives of the approximated field $u(\mathbf{x},\tau)$ are expressed in terms of the same nodal values as

$$u_{,k}(\mathbf{x},\tau) = \sum_{a=1}^{n} \hat{u}^a(\tau)\phi^a_{,k}(\mathbf{x}). \tag{43}$$

Substituting the approximation (43) into the definition of the bending moments (A.1) and then using $M_\alpha(\mathbf{x},\tau) = M_{\alpha\beta}(\mathbf{x},\tau)n_\beta(\mathbf{x})$, one obtains for $\mathbf{M}(\mathbf{x},\tau) = [M_1(\mathbf{x},\tau), M_2(\mathbf{x},\tau)]^{\mathrm{T}}$

$$\mathbf{M}(\mathbf{x},\tau) = \mathbf{N_1}\sum_{a=1}^{n}\mathbf{B}_1^a(\mathbf{x})\mathbf{w}^{*a}(\tau) + \mathbf{N_1}\sum_{a=1}^{n}\mathbf{B}_2^a(\mathbf{x})\mathbf{u}_0^{*a}(\tau) + \sum_{a=1}^{n}\mathbf{F}^a(\mathbf{x})\hat{\psi}_1^a(\tau) + \sum_{a=1}^{n}\mathbf{K}^a(\mathbf{x})\hat{\mu}_1^a(\tau), \tag{44}$$

where the vector $\mathbf{w}^{*a}(\tau)$ is defined as a column vector $\mathbf{w}^{*a}(\tau) = [\hat{w}_1^a(\tau), \hat{w}_2^a(\tau)]^{\mathrm{T}}$, the matrices $\mathbf{N}_1(\mathbf{x})$ are related to the normal vector $\mathbf{n}(\mathbf{x})$ on $\partial\Omega_s$ given by

$$\mathbf{N}_1(\mathbf{x}) = \begin{bmatrix} n_1 & 0 & n_2 \\ 0 & n_2 & n_1 \end{bmatrix}.$$

Also in equation (44), the matrices $\mathbf{B}_\alpha^a$ are represented by the gradients of the shape functions as

$$\mathbf{B}_1^a(\mathbf{x}) = \begin{bmatrix} (D_{11}+F_{12})\phi^a_{,1} & (D_{12}+F_{13})\phi^a_{,2} \\ (D_{12}+F_{22})\phi^a_{,1} & (D_{22}+F_{23})\phi^a_{,2} \\ \Delta_{11}\phi^a_{,2} & \Delta_{11}\phi^a_{,1} \end{bmatrix},$$
$$\mathbf{B}_2^a(\mathbf{x}) = \begin{bmatrix} G_{11}\phi^a_{,1} & G_{12}\phi^a_{,2} \\ G_{21}\phi^a_{,1} & G_{22}\phi^a_{,2} \\ \Gamma_{11}\phi^a_{,2} & \Gamma_{11}\phi^a_{,1} \end{bmatrix},$$

and

$$\mathbf{F}^a(\mathbf{x}) = \begin{bmatrix} F_{11}n_1\phi^a \\ F_{21}n_2\phi^a \end{bmatrix}, \qquad \mathbf{K}^a(\mathbf{x}) = \begin{bmatrix} K_{11}n_1\phi^a \\ K_{21}n_2\phi^a \end{bmatrix}. \tag{45}$$

Similarly one can obtain the approximation for the shear forces $\mathbf{Q}(\mathbf{x},\tau) = [Q_1(\mathbf{x},\tau), Q_2(\mathbf{x},\tau)]^{\mathrm{T}}$

$$\mathbf{Q}(\mathbf{x},\tau) = \mathbf{C}(\mathbf{x})\sum_{a=1}^{n}\left[\phi^a(\mathbf{x})\mathbf{w}^{*a}(\tau) + \mathbf{L}^a(\mathbf{x})\hat{w}_3^a(\tau)\right], \tag{46}$$

where

$$\mathbf{C}(\mathbf{x}) = \begin{bmatrix} C_1(\mathbf{x}) & 0 \\ 0 & C_2(\mathbf{x}) \end{bmatrix}, \qquad \mathbf{L}^a(\mathbf{x}) = \begin{bmatrix} \phi^a_{,1} \\ \phi^a_{,2} \end{bmatrix}.$$

The traction vector is approximated by

$$\mathbf{N}(\mathbf{x},\tau) = \mathbf{N_1}\sum_{a=1}^{n}\mathbf{G}^a(\mathbf{x})\mathbf{w}^{*a}(\tau) + \mathbf{N_1}\sum_{a=1}^{n}\mathbf{P}^a(\mathbf{x})\mathbf{u}_0^{*a}(\tau) + \sum_{a=1}^{n}\mathbf{S}^a(\mathbf{x})\hat{\psi}_1^a(\tau) + \sum_{a=1}^{n}\mathbf{J}^a(\mathbf{x})\hat{\mu}_1^a(\tau), \tag{47}$$

where

$$\mathbf{G}^a(\mathbf{x}) = \begin{bmatrix} (G_{11}+S_{12})\phi^a_{,1} & (G_{21}+S_{13})\phi^a_{,2} \\ (G_{12}+S_{23})\phi^a_{,1} & (G_{22}+S_{22})\phi^a_{,2} \\ \Gamma_{11}\phi^a_{,2} & \Gamma_{11}\phi^a_{,1} \end{bmatrix},$$

$$\mathbf{P}^a(\mathbf{x}) = \begin{bmatrix} P_{11}\phi^a_{,1} & P_{12}\phi^a_{,2} \\ P_{12}\phi^a_{,1} & P_{22}\phi^a_{,2} \\ \Gamma_{21}\phi^a_{,2} & \Gamma_{21}\phi^a_{,1} \end{bmatrix},$$

and

$$\mathbf{S}^a(\mathbf{x}) = \begin{bmatrix} S_{11}n_1\phi^a \\ S_{21}n_2\phi^a \end{bmatrix}, \qquad \mathbf{J}^a(\mathbf{x}) = \begin{bmatrix} J_{11}n_1\phi^a \\ J_{21}n_2\phi^a \end{bmatrix}.$$

Then, insertion of the MLS-discretized moment and force fields (44), (46) and (47) into the local integral equations (39)–(41) yields the discretized local integral equations

$$\begin{aligned}
&\sum_{a=1}^{n}\left[\int_{\partial\Omega_s^i}\mathbf{N}_1(\mathbf{x})\mathbf{B}_1^a(\mathbf{x})\,d\Gamma - \int_{\Omega_s^i}\mathbf{C}(\mathbf{x})\phi^a(\mathbf{x})\,d\Omega\right]\mathbf{w}^{*a}(\tau) \\
&\quad - \sum_{a=1}^{n} I_{M\alpha}\ddot{\mathbf{w}}^{*a}(\tau)\left(\int_{\Omega_s^i}\phi^a(\mathbf{x})\,d\Omega\right) \\
&\quad + \sum_{a=1}^{n}\left[\int_{\partial\Omega_s^i}\mathbf{N}_1(\mathbf{x})\mathbf{B}_2^a(\mathbf{x})\,d\Gamma\right]\mathbf{u}_0^{*a}(\tau) \\
&\quad + \sum_{a=1}^{n}\left[\int_{\partial\Omega_s^i}\mathbf{F}^a(\mathbf{x})\,d\Gamma\right]\hat{\psi}_1^a(\tau) \\
&\quad + \sum_{a=1}^{n}\left[\int_{\partial\Omega_s^i}\mathbf{K}^a(\mathbf{x})\,d\Gamma\right]\hat{\mu}_1^a(\tau) \\
&\quad - \sum_{a=1}^{n}\hat{w}_3^a(\tau)\left(\int_{\Omega_s^i}\mathbf{C}(\mathbf{x})\mathbf{K}^a(\mathbf{x})\,d\Omega\right) \\
&= -\int_{\Gamma_{sM}^i}\tilde{\mathbf{M}}(\mathbf{x},\tau)\,d\Gamma,
\end{aligned} \tag{48}$$

$$\begin{aligned}
&\sum_{a=1}^{n}\left(\int_{\partial\Omega_s^i}\mathbf{C}_n(\mathbf{x})\phi^a(\mathbf{x})\,d\Gamma\right)\mathbf{w}^{*a}(\tau) \\
&\quad + \sum_{a=1}^{n}\hat{w}_3^a(\tau)\left(\int_{\partial\Omega_s^i}\mathbf{C}_n(\mathbf{x})\mathbf{K}^a(\mathbf{x})\,d\Gamma\right) \\
&= -I_Q\sum_{a=1}^{n}\ddot{\hat{w}}_3^a(\tau)\left(\int_{\Omega_s^i}\phi^a(\mathbf{x})\,d\Omega\right) \\
&= -\int_{\Omega_s^i}q(\mathbf{x},\tau)\,d\Omega,
\end{aligned} \tag{49}$$

$$\begin{aligned}
&\sum_{a=1}^{n}\left[\int_{\partial\Omega_s^i}\mathbf{N}_1(\mathbf{x})\mathbf{G}^a(\mathbf{x})\,d\Gamma\right]\mathbf{w}^{*a}(\tau) \\
&\quad - \sum_{a=1}^{n} I_Q\ddot{\mathbf{u}}_0^{*a}(\tau)\left(\int_{\Omega_s^i}\phi^a(\mathbf{x})\,d\Omega\right) \\
&\quad + \sum_{a=1}^{n}\left[\int_{\partial\Omega_s^i}\mathbf{N}_1(\mathbf{x})\mathbf{P}^a(\mathbf{x})\,d\Gamma\right]\mathbf{u}_0^{*a}(\tau) \\
&\quad + \sum_{a=1}^{n}\left[\int_{\partial\Omega_s^i}\mathbf{S}^a(\mathbf{x})\,d\Gamma\right]\hat{\psi}_1^a(\tau) \\
&\quad + \sum_{a=1}^{n}\left[\int_{\partial\Omega_s^i}\mathbf{J}^a(\mathbf{x})\,d\Gamma\right]\hat{\mu}_1^a(\tau) \\
&= -\int_{\Gamma_{sN}^i}\tilde{\mathbf{N}}(\mathbf{x},\tau)\,d\Gamma,
\end{aligned} \tag{50}$$

in which $\tilde{\mathbf{M}}(\mathbf{x},\tau)$ represent the prescribed bending moments on Γ_{sM}^i, $\tilde{\mathbf{N}}(\mathbf{x},\tau)$ is the prescribed traction vector on Γ_{sN}^i and

$$\mathbf{C}_n(\mathbf{x}) = (n_1, n_2)\begin{pmatrix} C_1 & 0 \\ 0 & C_2 \end{pmatrix} = (C_1n_1, C_2n_2).$$

Equations (48)–(50) are considered on the subdomains adjacent to the interior nodes $\mathbf{x}^i$. For the source point $\mathbf{x}^i$ located on the global boundary Γ the boundary of the subdomain $\partial\Omega_s^i$ is decomposed into L_s^i and Γ_{sM}^i (part of the global boundary with the prescribed bending moment) or Γ_{sN}^i with the prescribed traction vector.

If the MEE layer is used as a sensor, then the laminated plate is under a mechanical load. Then, the system of the LIE (48)–(50) has to be supplemented by equations (26) and (27) representing vanishing electrical displacement and magnetic induction on the top surface of the plate.

It should be noted here that there are neither Lagrange multipliers nor penalty parameters introduced into the local weak-forms (32)–(34) because the essential boundary conditions on Γ_{sw}^i (part of the global boundary with prescribed rotations or displacements) and Γ_{su}^i (part of the global boundary with prescribed in-plane displacements) can be imposed directly, using the interpolation approximation (42)

$$\sum_{a=1}^{n}\phi^a(\mathbf{x}^i)\hat{u}^a(\tau) = \tilde{u}(\mathbf{x}^i,\tau) \qquad \text{for } \mathbf{x}^i \in \Gamma_{sw}^i \quad \text{or} \quad \Gamma_{su}^i, \tag{51}$$

where $\tilde{u}(\mathbf{x}^i,\tau)$ is the prescribed value on the boundary Γ_{sw}^i and Γ_{su}^i. For a clamped plate the rotations and deflection are vanishing on the fixed edge, and equation (51) is used at all the boundary nodes in such a case. However, for a simply supported plate only the deflection $\tilde{w}_3(\mathbf{x}^i,\tau)$, the bending moment and normal stress are prescribed, while the rotations and in-plane displacements are unknown. Then, the approximation formulas (44) and (47) are applied to the nodes lying on the global boundary.

$$\begin{aligned}
\tilde{\mathbf{M}}(\mathbf{x}^i,\tau) &= \mathbf{N_1}\sum_{a=1}^{n}\mathbf{B}_1^a(\mathbf{x}^i)\mathbf{w}^{*a}(\tau) \\
&\quad + \mathbf{N_1}\sum_{a=1}^{n}\mathbf{B}_2^a(\mathbf{x}^i)\mathbf{u}_0^{*a}(\tau) + \sum_{a=1}^{n}\mathbf{F}^a(\mathbf{x}^i)\hat{\psi}_1^a(\tau) \\
&\quad + \sum_{a=1}^{n}\mathbf{K}^a(\mathbf{x}^i)\hat{\mu}_1^a(\tau), \qquad \text{for } \mathbf{x}^i \in \Gamma_{sM}^i
\end{aligned} \tag{52}$$

$$\tilde{\mathbf{N}}(\mathbf{x}^i,\tau) = \mathbf{N_1}\sum_{a=1}^{n}\mathbf{G}^a(\mathbf{x}^i)\mathbf{w}^{*a}(\tau) + \mathbf{N_1}\sum_{a=1}^{n}\mathbf{P}^a(\mathbf{x}^i)\mathbf{u_0}^{*a}(\tau) + \sum_{a=1}^{n}\mathbf{S}^a(\mathbf{x}^i)\hat{\psi}_1^a(\tau) + \sum_{a=1}^{n}\mathbf{J}^a(\mathbf{x}^i)\hat{\mu}_1^a(\tau), \qquad \text{for } \mathbf{x}^i \in \Gamma_{sN}^i. \tag{53}$$

If the MEE layer in the laminated plate is used as an actuator, then the electric and magnetic potentials are prescribed on the top of the plate. Both potentials can be expressed through the mechanical quantities given by equations (30) and (31). Then, the total unknowns are reduced to 5 unknown quantities $(w_1, w_2, w_3, u_0, v_0)$ and the local integral equations have the following form

$$\begin{aligned}
&\sum_{a=1}^{n}\left[\int_{\partial\Omega_s^i}\mathbf{N}_1(\mathbf{x})\mathbf{B}_1^a(\mathbf{x})\,d\Gamma - \int_{\Omega_s^i}\mathbf{C}(\mathbf{x})\phi^a(\mathbf{x})\,d\Omega\right]\mathbf{w}^{*a}(\tau)\\
&\quad - \sum_{a=1}^{n} I_{M\alpha}\ddot{\mathbf{w}}^{*a}(\tau)\left(\int_{\Omega_s^i}\phi^a(\mathbf{x})\,d\Omega\right)\\
&\quad + \sum_{a=1}^{n}\left[\int_{\partial\Omega_s^i}\mathbf{N}_1(\mathbf{x})\mathbf{B}_2^a(\mathbf{x})\,d\Gamma\right]\mathbf{u}_0^{*a}(\tau)\\
&\quad + \int_{\partial\Omega_s^i}\tilde{\psi}(\mathbf{x},\tau)\mathbf{F}(\mathbf{x})\,d\Gamma\\
&\quad - \sum_{a=1}^{n}\left[\int_{\partial\Omega_s^i}\mathbf{F}_{\mathbf{act}}^{\mathbf{a}}(\mathbf{x})\,d\Gamma\right]\mathbf{w}^{*a}(\tau)\\
&\quad + \int_{\partial\Omega_s^i}\tilde{\mu}(\mathbf{x},\tau)\mathbf{K}(\mathbf{x})\,d\Gamma\\
&\quad - \sum_{a=1}^{n}\left[\int_{\partial\Omega_s^i}\mathbf{K}_{\mathbf{act}}^{\mathbf{a}}(\mathbf{x})\,d\Gamma\right]\mathbf{w}^{*a}(\tau)\\
&\quad - \sum_{a=1}^{n}\hat{w}_3^a(\tau)\left(\int_{\Omega_s^i}\mathbf{C}(\mathbf{x})\mathbf{K}^a(\mathbf{x})\,d\Omega\right)\\
&= -\int_{\Gamma_{sM}^i}\tilde{\mathbf{M}}(\mathbf{x},\tau)\,d\Gamma,
\end{aligned} \tag{54}$$

$$\begin{aligned}
&\sum_{a=1}^{n}\left(\int_{\partial\Omega_s^i}\mathbf{C}_n(\mathbf{x})\phi^a(\mathbf{x})\,d\Gamma\right)\mathbf{w}^{*a}(\tau)\\
&\quad + \sum_{a=1}^{n}\hat{w}_3^a(\tau)\left(\int_{\partial\Omega_s^i}\mathbf{C}_n(\mathbf{x})\mathbf{K}^a(\mathbf{x})\,d\Gamma\right)\\
&= -I_Q\sum_{a=1}^{n}\ddot{\hat{w}}_3^a(\tau)\left(\int_{\Omega_s^i}\phi^a(\mathbf{x})\,d\Omega\right)\\
&= -\int_{\Omega_s^i} q(\mathbf{x},\tau)\,d\Omega,
\end{aligned} \tag{55}$$

$$\begin{aligned}
&\sum_{a=1}^{n}\left[\int_{\partial\Omega_s^i}\mathbf{N}_1(\mathbf{x})\mathbf{G}^a(\mathbf{x})\,d\Gamma\right]\mathbf{w}^{*a}(\tau)\\
&\quad - \sum_{a=1}^{n} I_Q\ddot{\mathbf{u}}_0^{*a}(\tau)\left(\int_{\Omega_s^i}\phi^a(\mathbf{x})\,d\Omega\right)\\
&\quad + \sum_{a=1}^{n}\left[\int_{\partial\Omega_s^i}\mathbf{N}_1(\mathbf{x})\mathbf{P}^a(\mathbf{x})\,d\Gamma\right]\mathbf{u}_0^{*a}(\tau)\\
&\quad + \int_{\partial\Omega_s^i}\tilde{\psi}(\mathbf{x},\tau)\mathbf{S}(\mathbf{x})\,d\Gamma\\
&\quad - \sum_{a=1}^{n}\left[\int_{\partial\Omega_s^i}\mathbf{S}_{\mathbf{act}}^{\mathbf{a}}(\mathbf{x})\,d\Gamma\right]\mathbf{w}^{*a}(\tau)\\
&\quad + \int_{\partial\Omega_s^i}\tilde{\mu}(\mathbf{x},\tau)\mathbf{J}(\mathbf{x})\,d\Gamma\\
&\quad - \sum_{a=1}^{n}\left[\int_{\partial\Omega_s^i}\mathbf{J}_{\mathbf{act}}^{\mathbf{a}}(\mathbf{x})\,d\Gamma\right]\mathbf{w}^{*a}(\tau)\\
&\quad = -\int_{\Gamma_{sN}^i}\tilde{\mathbf{N}}(\mathbf{x},\tau)\,d\Gamma,
\end{aligned} \tag{56}$$

where

$$\mathbf{F}(\mathbf{x}) = \begin{bmatrix} F_{11}n_1 \\ F_{21}n_2 \end{bmatrix}, \qquad \mathbf{K}(\mathbf{x}) = \begin{bmatrix} K_{11}n_1 \\ K_{21}n_2 \end{bmatrix},$$

$$\mathbf{S}(\mathbf{x}) = \begin{bmatrix} S_{11}n_1 \\ S_{21}n_2 \end{bmatrix}, \qquad \mathbf{J}(\mathbf{x}) = \begin{bmatrix} J_{11}n_1 \\ J_{21}n_2 \end{bmatrix},$$

$$\begin{aligned}
&\mathbf{F}_{\mathbf{act}}^{\mathbf{a}}(\mathbf{x})\\
&\quad = \frac{h_2^2}{2(\alpha_{33}\alpha_{33} - \gamma_{33}h_{33})}\\
&\qquad \times \begin{bmatrix} F_{11}n_1(\alpha_{33}d_{31} - e_{31}\gamma_{33})\phi_{,1}^a & F_{11}n_1(\alpha_{33}d_{32} - e_{32}\gamma_{33})\phi_{,2}^a \\ F_{21}n_2(\alpha_{33}d_{31} - e_{31}\gamma_{33})\phi_{,1}^a & F_{21}n_2(\alpha_{33}d_{32} - e_{32}\gamma_{33})\phi_{,2}^a \end{bmatrix},
\end{aligned}$$

$$\begin{aligned}
&\mathbf{K}_{\mathbf{act}}^{\mathbf{a}}(\mathbf{x})\\
&\quad = \frac{h_2^2}{2(\alpha_{33}\alpha_{33} - \gamma_{33}h_{33})}\\
&\qquad \times \begin{bmatrix} K_{11}n_1(\alpha_{33}e_{31} - d_{31}h_{33})\phi_{,1}^a & K_{11}n_1(\alpha_{33}e_{32} - d_{32}h_{33})\phi_{,2}^a \\ K_{21}n_2(\alpha_{33}e_{31} - d_{31}h_{33})\phi_{,1}^a & K_{21}n_2(\alpha_{33}e_{32} - d_{32}h_{33})\phi_{,2}^a \end{bmatrix},
\end{aligned}$$

$$\begin{aligned}
&\mathbf{S}_{\mathbf{act}}^{\mathbf{a}}(\mathbf{x})\\
&\quad = \frac{h_2^2}{2(\alpha_{33}\alpha_{33} - \gamma_{33}h_{33})}\\
&\qquad \times \begin{bmatrix} S_{11}n_1(\alpha_{33}d_{31} - e_{31}\gamma_{33})\phi_{,1}^a & S_{11}n_1(\alpha_{33}d_{32} - e_{32}\gamma_{33})\phi_{,2}^a \\ S_{21}n_2(\alpha_{33}d_{31} - e_{31}\gamma_{33})\phi_{,1}^a & S_{21}n_2(\alpha_{33}d_{32} - e_{32}\gamma_{33})\phi_{,2}^a \end{bmatrix},
\end{aligned}$$

$$\begin{aligned}
&\mathbf{J}_{\mathbf{act}}^{\mathbf{a}}(\mathbf{x})\\
&\quad = \frac{h_2^2}{2(\alpha_{33}\alpha_{33} - \gamma_{33}h_{33})}\\
&\qquad \times \begin{bmatrix} J_{11}n_1(\alpha_{33}e_{31} - d_{31}h_{33})\phi_{,1}^a & J_{11}n_1(\alpha_{33}e_{32} - d_{32}h_{33})\phi_{,2}^a \\ J_{21}n_2(\alpha_{33}e_{31} - d_{31}h_{33})\phi_{,1}^a & J_{21}n_2(\alpha_{33}e_{32} - d_{32}h_{33})\phi_{,2}^a \end{bmatrix}.
\end{aligned}$$

Collecting the discretized local boundary-domain integral equations together with the discretized boundary conditions for the generalized displacements, bending moment and traction vector, one obtains a complete system of ordinary differential equations, which can be rearranged in such a way that all known quantities are on the rhs. Thus, in matrix form the system becomes

$$\mathbf{A}\ddot{\mathbf{x}} + \mathbf{C}\mathbf{x} = \mathbf{Y}. \tag{57}$$

The system of ordinary differential equations is solved by the Houbolt method [32]. The acceleration $\ddot{\mathbf{x}}$ is expressed as

$$\ddot{\mathbf{x}}_{\tau+\Delta\tau} = \frac{2\mathbf{x}_{\tau+\Delta\tau} - 5\mathbf{x}_{\tau} + 4\mathbf{x}_{\tau-\Delta\tau} - \mathbf{x}_{\tau-2\Delta\tau}}{\Delta\tau^2}, \quad (58)$$

where $\Delta\tau$ is the time step.

Substituting equation (58) into (57), we obtain the following system of algebraic equations for the unknowns $\mathbf{x}_{\tau+\Delta\tau}$

$$\left[\frac{2}{\Delta\tau^2}\mathbf{A} + \mathbf{C}\right]\mathbf{x}_{\tau+\Delta\tau} = \frac{1}{\Delta\tau^2}5\mathbf{A}\mathbf{x}_{\tau} + \mathbf{A}\frac{1}{\Delta\tau^2}\{-4\mathbf{x}_{\tau-\Delta\tau} + \mathbf{x}_{\tau-2\Delta\tau}\} + \mathbf{Y}. \quad (59)$$

4. Numerical examples

A two-layered square plate with a side length $a = 0.254$ m is analyzed to verify the proposed computational method. The total thickness of the plate is $h = 0.012$ m. To test the proposed computational method, homogeneous properties are considered in the first step for the elastic layer. The elastic layer #1 has the plate thickness $h_1 = 3h/4$. Two different materials are used for the layer #1: (1) In the first case the material is denoted as $\#B$ and its material coefficients are considered as:

$$c_{11}^{(1B)} = 10.989 \times 10^{10}\ \mathrm{N\,m^{-2}},$$
$$c_{12}^{(1B)} = 3.297 \times 10^{10}\ \mathrm{N\,m^{-2}},$$
$$c_{22}^{(1B)} = 10.989 \times 10^{10}\ \mathrm{N\,m^{-2}},$$
$$c_{66}^{(1B)} = 3.846 \times 10^{10}\ \mathrm{N\,m^{-2}},$$
$$c_{44}^{(1B)} = c_{55}^{(1B)} = 3.846 \times 10^{10}\ \mathrm{N\,m^{-2}}.$$

(2) To analyze the influence of the stiffness matrix of the elastic layer on the deflection and the induced electric and magnetic potentials in the MEE layer, we have considered also an elastic layer with lower stiffness parameters. This material is denoted as $\#T$, and its parameters are given by

$$c_{ij}^{(1T)} = c_{ij}^{(1B)}/2.$$

The second layer with thickness $h_2 = h/4$ has the MEE properties and the material parameters correspond to $BaTiO_3$–$CoFe_2O_4$ [41]:

$$c_{11}^{(2)} = c_{22}^{(2)} = 22.6 \times 10^{10}\ \mathrm{N\,m^{-2}},$$
$$c_{12}^{(2)} = 12.4 \times 10^{10}\ \mathrm{N\,m^{-2}},$$
$$c_{33}^{(2)} = 21.6 \times 10^{10}\ \mathrm{N\,m^{-2}},$$
$$c_{66}^{(2)} = 5.1 \times 10^{10}\ \mathrm{N\,m^{-2}},$$
$$c_{44}^{(2)} = c_{55}^{(2)} = 4.3 \times 10^{10}\ \mathrm{N\,m^{-2}},$$
$$e_{31}^{(2)} = e_{32}^{(2)} = -2.2\ \mathrm{C\,m^{-2}}, \qquad e_{15}^{(2)} = 5.8\ \mathrm{C\,m^{-2}},$$
$$h_{33}^{(2)} = 6.35 \times 10^{-9}\ \mathrm{C\,(V\,m)^{-1}},$$
$$h_{11}^{(2)} = 5.64 \times 10^{-9}\ \mathrm{C\,(V\,m)^{-1}},$$
$$d_{31}^{(2)} = d_{32}^{(2)} = 290.2\ \mathrm{N\,A^{-1}\,m^{-1}},$$

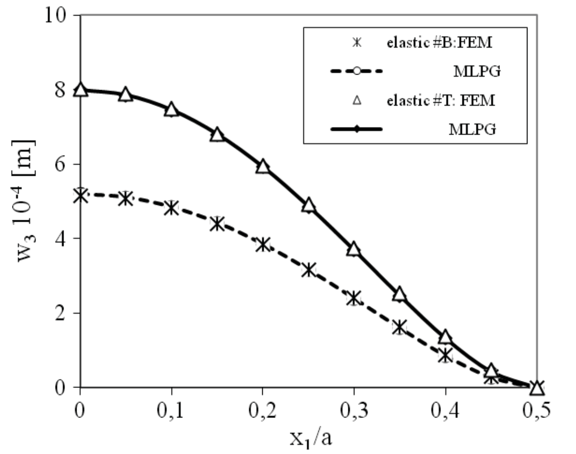

Figure 2. Variation of the deflection with the x_1-coordinate for the clamped plate.

$$d_{33}^{(2)} = 350\ \mathrm{N\,A^{-1}\,m^{-1}}, \qquad d_{15}^{(2)} = 275\ \mathrm{N\,A^{-1}\,m^{-1}},$$
$$\alpha_{11}^{(2)} = 5.367 \times 10^{-12}\ \mathrm{N\,s\,(V\,C)^{-1}},$$
$$\alpha_{33}^{(2)} = 2737.5 \times 10^{-12}\ \mathrm{N\,s\,(V\,C)^{-1}},$$
$$\gamma_{11}^{(2)} = 297 \times 10^{-6}\ \mathrm{Wb\,(A\,m)^{-1}},$$
$$\gamma_{33}^{(2)} = 83.5 \times 10^{-6}\ \mathrm{Wb\,(A\,m)^{-1}}, \qquad \rho = 7500\ \mathrm{kg\,m^{-3}}.$$

A uniform load with intensity $q = 2.0 \times 10^6\ \mathrm{N\,m^{-2}}$ is applied on the top surface of the layered plate. A vanishing electric displacement and magnetic induction are prescribed on the top surface. In our numerical calculations, 441 nodes with a regular distribution were used for the approximation of the rotations, the deflection, in-plane displacements, electric and magnetic potentials in the neutral plane. The origin of the coordinate system is located at the center of the plate.

First, clamped boundary conditions have been considered. The variation of the deflection with the x_1-coordinate at $x_2 = 0$ of the plate is presented in figure 2. The numerical results are compared with the results obtained by the COMSOL code as 3D analysis with 3364 quadratic elements for a quarter of the plate. Our numerical results are in a very good agreement with those obtained by the FEM. The relative error of the maximal deflection is 0.32% for material $\#T$ and 0.65% for material $\#B$ by our MLPG if COMSOL results with a very fine mesh are considered as the correct ones. One can observe that the deflection value is reduced for the elastic plate corresponding to material $\#B$ with respect to material $\#T$.

The induced electric potential ψ on the top surface of the plate is presented in figure 3. It is observed that there is a quite good agreement between the MLPG and FEM results. The relative error of the maximal electric potential is 0.7% for material $\#T$ and 1.5% for material $\#B$. Similarly, the relative error of the maximal magnetic potential is 1.7% for material $\#T$ and 1.8% for material $\#B$. One can see that material parameters of the elastic layer have a small influence on the induced potential. At the material $\#T$ the maximal deflection is reduced about 54%, however, the electric potential is reduced only 10%. A similar conclusion can be done for the

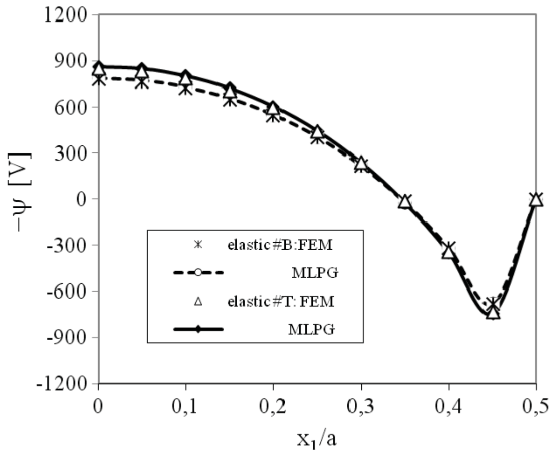

Figure 3. Variation of the electric potential with the x_1-coordinate for the clamped plate.

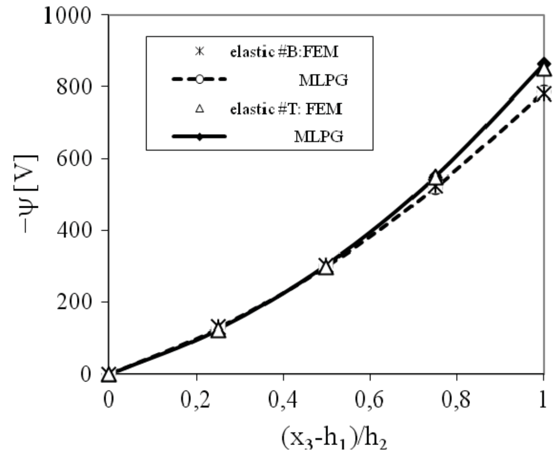

Figure 5. Variation of the electric potential along the thickness of the MEE layer for the clamped plate.

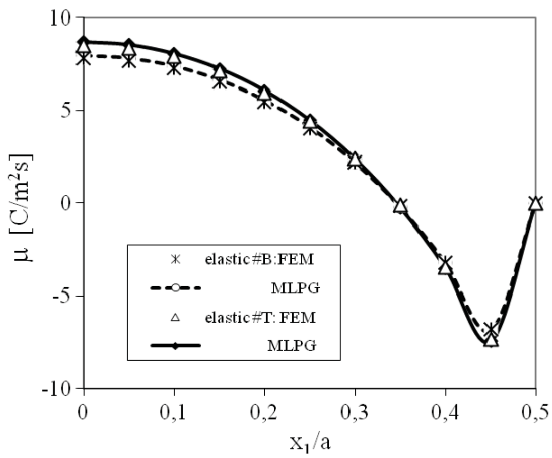

Figure 4. Variation of the magnetic potential with the x_1-coordinate for the clamped plate.

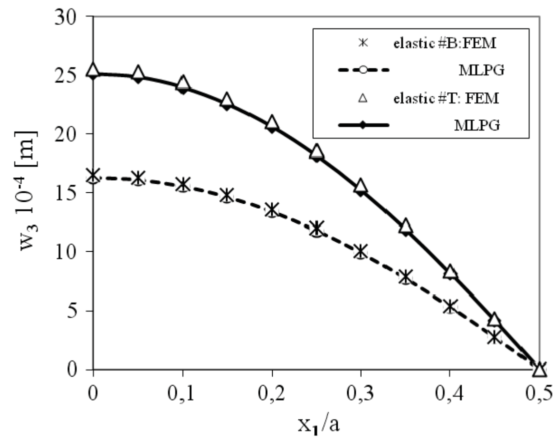

Figure 6. Variation of the deflection with the x_1-coordinate for the simply supported plate.

magnetic potential presented in figure 4. The variations of both potentials with x_1-coordinate are very similar. It is given by the ratio of piezomagnetic and piezoelectric coefficients, since $B_3/D_3 = d_{31}/e_{31}$. Then, it is valid that

$$\frac{H_3}{E_3} = \frac{B_3}{D_3}\frac{h_{33}}{\gamma_{33}} = \frac{d_{31}h_{33}}{\gamma_{33}e_{31}}. \tag{60}$$

The variation of the electric potential with x_3-coordinate is given in figure 5. We have obtained a good agreement between the MLPG and FEM results for the quadratic approximation of the electric potential along x_3. If we use only a linear approximation we get a discrepancy on the top surface of about 37%. For a very thin MEE layer we expect a smaller discrepancy even for a linear approximation.

Then, a simply supported plate with the same material properties, geometry and loading is analyzed. The variation of the deflection with the x_1-coordinate at $x_2 = 0$ of the plate is presented in figure 6. The maximal deflection is reduced about 54% for the layered plate if the stiffness parameters in the elastic layer are doubled. The reduction is similar to the case of the clamped plate. The variations of the electric and magnetic potentials with the x_1-coordinate are presented in figures 7 and 8. The relative errors of the maximal deflection, electric potential and magnetic potential are, respectively, 1.8%, 1.6% and 1.5% for material #T. The induced potentials for the simply supported plate are significantly larger than for the clamped plate. It is due to larger deformations for the simply supported plate. Since the gradient of the deflection is monotonically growing with x_1-coordinate for the simply supported plate, the electric potential on the whole interval x_1 is negative. It is not valid for the clamped plate. Again the shapes of both curves of potentials are very similar and the quantities are proportional to the ratio given by (60).

We now analyze the influence of the material gradation on the deflection and the electric and magnetic potentials, if functionally graded material properties are considered for the elastic plate described by equation (20). On the top surface of the elastic plate (layer #1) ($x_3 = h_1$) the material properties correspond to material #T from the previous analysis. On the bottom surface of the plate the material properties correspond to material #B. It is obvious

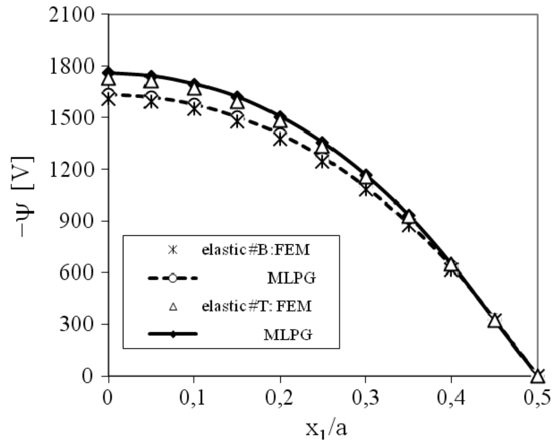

Figure 7. Variation of the electric potential with the x_1-coordinate for the simply supported plate.

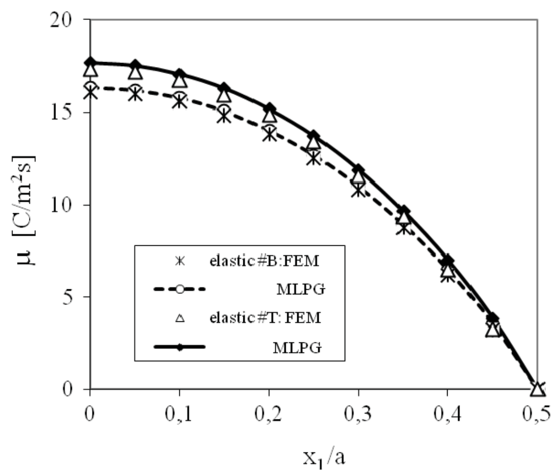

Figure 8. Variation of the magnetic potential with the x_1-coordinate for the simply supported plate.

that if exponent $n = 0$, we have homogeneous properties in the plate corresponding to material #*T*, and that if the exponent approaches infinity, the material properties are almost homogeneous, corresponding to material #*B*. Variations of the deflection with the x_1-coordinate for the clamped plate are presented in figure 9. One can observe that deflection for the FGM plate with exponent $n = 1$ is close to the homogeneous plate corresponding to material #*B*. It is due to the fact that material properties far from the neutral plane can have a strong influence on the deflection value.

The variations of the electric and magnetic potentials with the x_1-coordinate are presented in figures 10 and 11. The potentials for the FGM plate lie between the two potentials corresponding to the extreme cases given by material properties on the top and bottom of the elastic case. We have seen that the elastic material parameters have only a slight influence on the induced potentials for homogeneous plates.

The simply supported plate with functionally graded material properties for the elastic plate is analyzed too. The

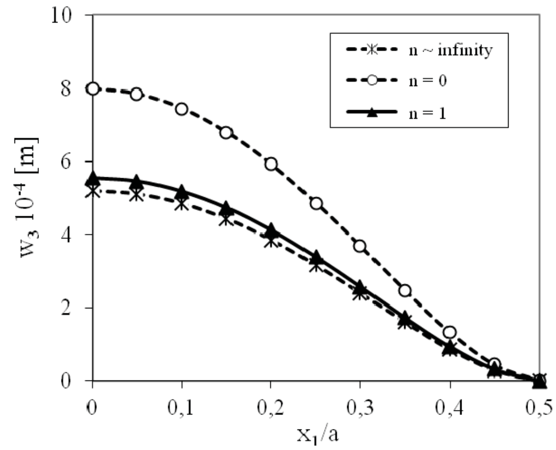

Figure 9. The influence of the material gradation on the deflection of the clamped plate.

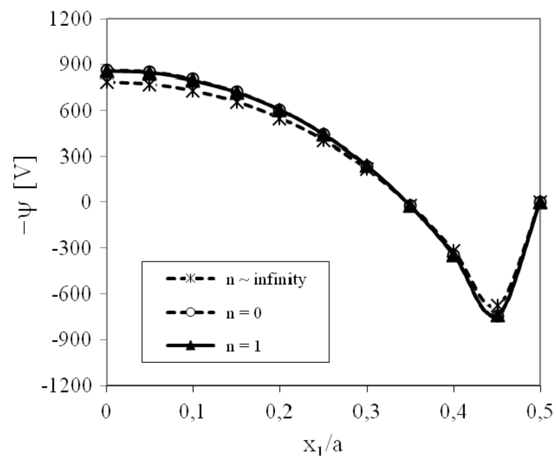

Figure 10. The influence of the material gradation on the electric potential of the clamped plate.

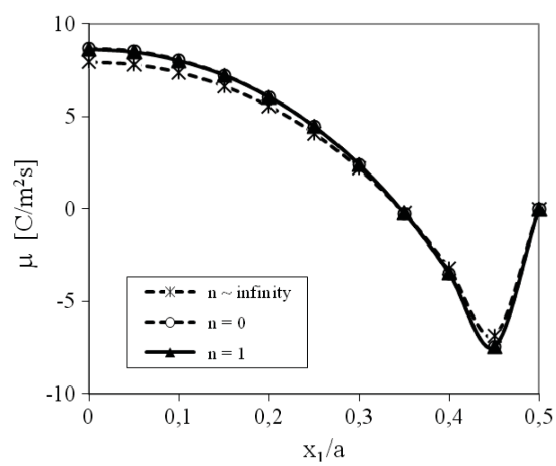

Figure 11. The influence of the material gradation on the magnetic potential of the clamped plate.

plate deflections are given in figure 12. We can make a similar conclusion on the influence of material gradation in this case as has been done for the clamped plate. The variations of the

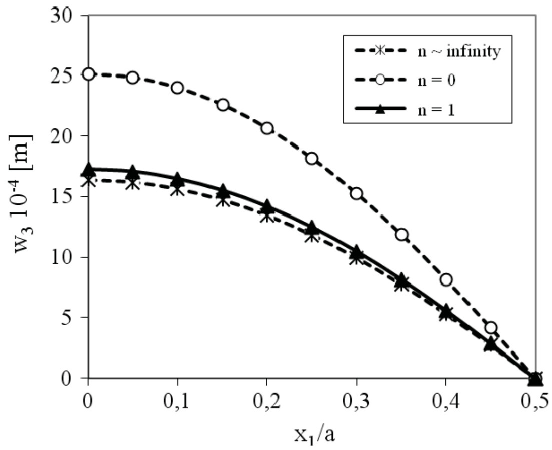

Figure 12. The influence of the material gradation on the deflection of the simply supported plate.

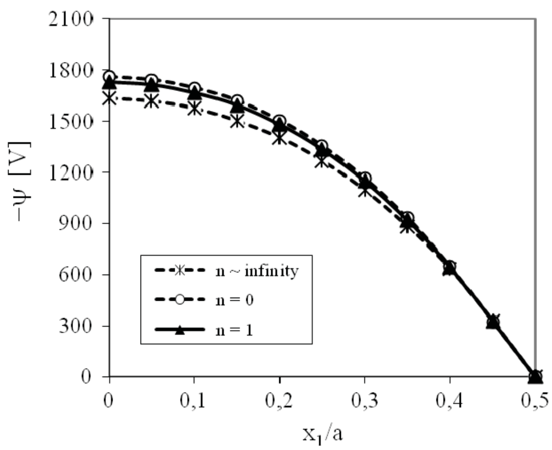

Figure 13. The influence of the material gradation on the electric potential of the simply supported plate.

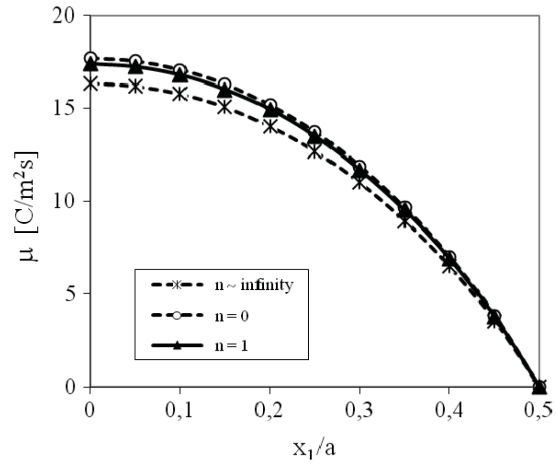

Figure 14. The influence of the material gradation on the magnetic potential of the simply supported plate.

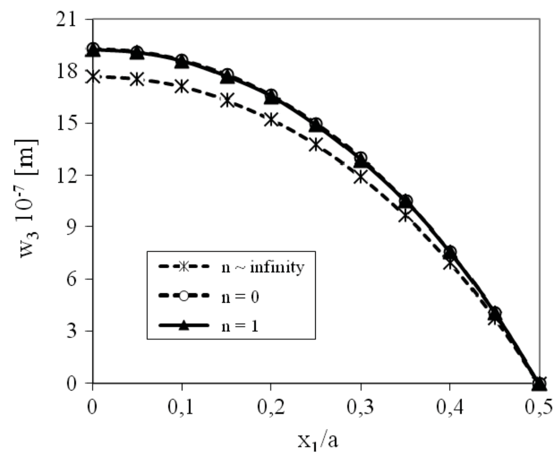

Figure 15. Variation of the deflection with the x_1-coordinate for the simply supported plate with prescribed electric potential.

electric and magnetic potentials are presented in figures 13 and 14.

We assume now that the MEE layer on the top surface is used as an actuator. Then, the electric potential is prescribed on the top surface, $\tilde{\psi} = 1000$ V. The magnetic potential is vanishing. Geometrical and material parameters are the same as in the previous example. The variation of the deflection along x_1 for the simply supported layered plate is presented in figure 15. In this case the deflection for the FGM plate is closer to the homogeneous plate with material properties corresponding to material #2 (lower stiffness). An opposite phenomenon is observed for the plate under a mechanical load. For a larger stiffness there is a tendency to decrease the gradients of rotations occurring in equations (30) and (31). Then, the values ψ_1 and μ_1 become larger. Therefore, the decrease of the deflection is eliminated by the increase of the efficient load.

In the previous example we have considered a pure electrical load. It is interesting to investigate also a combined electromagnetic load. For this purpose we introduce a non-dimensional parameter

$$\beta = \frac{d_{31}\tilde{\mu}}{e_{31}\tilde{\psi}} \tag{61}$$

where $\beta = 0$ corresponds to a pure electrical load, and for $\beta = 1$ we have $\tilde{\mu} = e_{31}\tilde{\psi}/d_{31}$ representing a ratio between the electric and magnetic effects. The influence of the combined electromagnetic load on the deflection is presented in figure 16.

Stationary conditions have been considered in the previous numerical example. If a finite velocity of elastic waves is considered, the acceleration term is included into the governing equations (23)–(25). The mass density $\rho = 7500$ kg m^{-3} is considered to be same for both elastic and MEE materials. Numerical calculations are carried out for a time step $\Delta\tau = 0.2 \times 10^{-4}$ s. The central plate deflection is normalized by the static deflection corresponding to the elastic material #*B*, $w_3^{\mathrm{stat}} = 0.1771 \times 10^{-5}$ m (see figure 15). The time variations of the normalized central deflections are

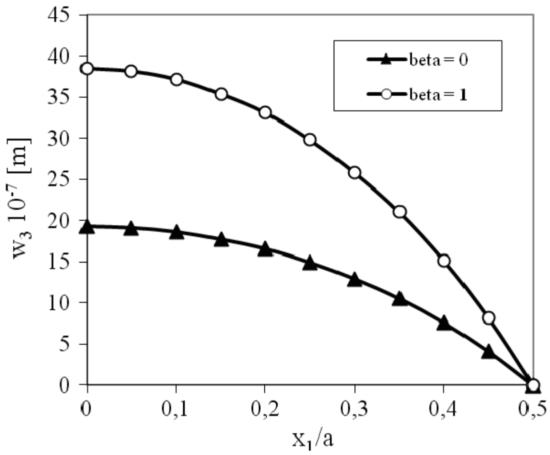

Figure 16. Variation of the deflection with the x_1-coordinate for the simply supported plate with combined electromagnetic load.

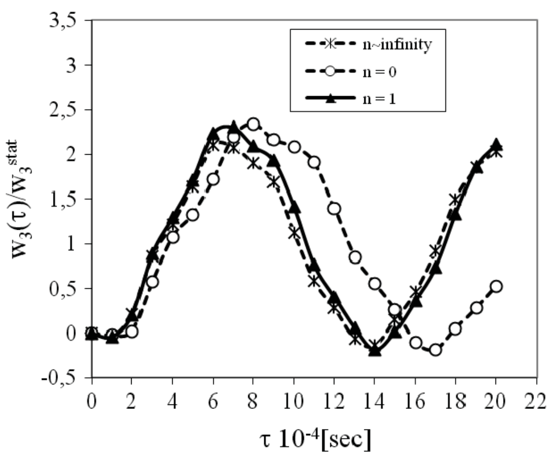

Figure 17. Time variation of the deflection at the center of a simply supported plate subjected to a suddenly applied electric potential.

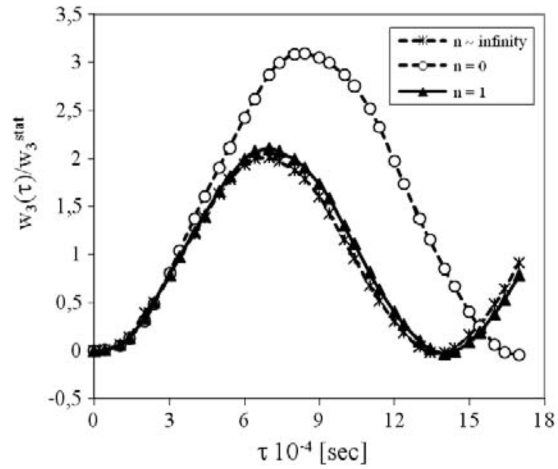

Figure 18. Time variation of the deflection at the center of a simply supported square plate subjected to a suddenly applied mechanical load.

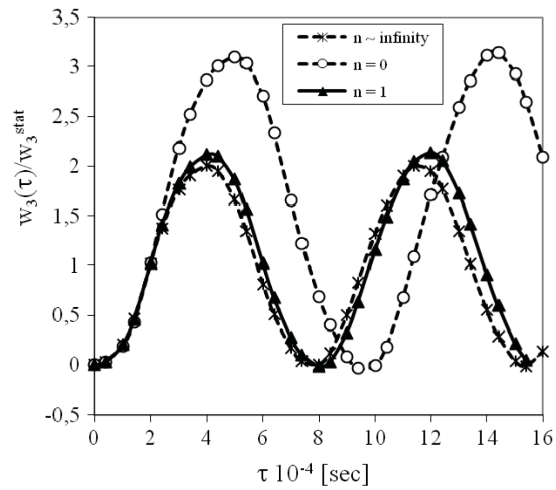

Figure 19. Time variation of the deflection at the center of a clamped laminated plate subjected to a suddenly applied load.

given in figure 17. One can observe a shift of the peak value for the stiffer material to shorter instants due to higher elastic wave velocities than in the material with lower stiffness (material #*T*). The peak value grows as the stiffness of the plate decreases.

The same plate with simply supported boundary conditions under an impact mechanical load with Heaviside time variation is analyzed too. The time variation of the central deflection is presented in figure 18. Deflections are normalized by the static deflection corresponding to material #*B*, $w_3^{\text{stat}} = 0.1634 \times 10^{-2}$ m. The peak value of the deflection for material #*T* (lower stiffness) is significantly large than for the plate with large stiffness. The deflection for the FGM plate is close to the value corresponding to the material #*B*. It is similar to a static case.

Finally, a clamped laminated square plate under a uniform impact load is analyzed, as shown in figure 19. The deflection values are normalized by the corresponding static central deflection $w_3^{\text{stat}} = 0.519 \times 10^{-3}$ m (corresponding to material #*B*). The peaks of the deflection amplitudes are shifted to shorter time instants for the laminated plate with a larger flexural rigidity. Since the mass density is the same for both elastic materials, the wave velocity is higher for the elastic plate with higher Young's moduli. The peak values are reached in shorter time instants for the clamped than for simply supported plate.

5. Conclusions

The meshless local Petrov–Galerkin method is developed for bending analyses of FGM plates with integrated MEE sensor and actuator layer. The formulation based on the shear deformation plate theory can be applied also for moderately thick plates. A polynomial variation of material properties along the FGM plate thickness is applied in numerical examples. However, the present computational method can be used for a general spatial variation of material properties. The electric and magnetic intensity vectors are assumed only in the plate thickness direction due to the assumption of a thin MEE layer. The Reissner–Mindlin theory reduces the original three-dimensional (3D) thick-plate problem to a 2D problem. Nodal points are randomly distributed over the mean surface of the considered plate. Each node is the center of a circle surrounding this node. The weak-form on small subdomains with a Heaviside step function as the test functions is applied to derive local integral equations. After performing the spatial MLS approximation, a system of ordinary differential equations for certain nodal unknowns is obtained. Then, the system of second-order ordinary differential equations resulting from the equations of motion is solved by the Houbolt finite-difference scheme as a time-stepping method.

Stationary and impact boundary conditions are considered in the numerical analyses. The influence of the material gradation on the plate deflection or on the induced potentials is shown. For instance, the induced potential for the simply supported plate is approximately twice as large as that for the clamped plate. This and other numerical results in the paper should be important for suitable design of a sensor or actuator using the MEE layer for efficient active control. The influence of both material gradation and mechanical boundary conditions on the design should be considered.

It is demonstrated numerically that the results obtained by the proposed MLPG method are reliable. Numerical results for homogeneous materials are compared with those obtained by the 3D FEM analyses. The agreement of our numerical results with those obtained by the COMSOL computer code is also very good. However, the 3D FEM analysis needs significantly more degrees of freedom than that based on the present in-plane formulation.

Acknowledgments

The authors acknowledge support by the Slovak Science and Technology Assistance Agency registered under number APVV-0014-10. The authors also gratefully acknowledge the financial assistance of the European Regional Development Fund (ERDF) under the Operational Programme Research and Development/Measure 4.1 Support of Networks of Excellence in Research and Development as the Pillars of Regional Development and Support to International Cooperation in the Bratislava region/Project No. 26240120020 Building the Centre of Excellence for Research and Development of Structural Composite Materials—2nd stage.

Appendix A. Detailed expressions for M_{ij}, N_{ij} and Q_i $(i, j = 1, 2)$

$$
\begin{aligned}
M_{11}(\mathbf{x},\tau) &= \sum_{k=1}^{2}\int_{z_k}^{z_{k+1}} \{c_{11}^{(k)}[(z-z_{011})w_{1,1}+u_{0,1}] \\
&\quad + c_{12}^{(k)}\,[(z-z_{022})w_{2,2}+v_{0,2}] \\
&\quad - e_{31}^{(k)}E_3 - d_{31}^{(k)}H_3\}(z-z_{011})\,\mathrm{d}z \\
&= D_{11}w_{1,1}+G_{11}u_{0,1}+D_{12}w_{2,2}+G_{12}v_{0,2} \\
&\quad + F_{11}\psi_1+F_{12}w_{1,1}+F_{13}w_{2,2}+K_{11}\mu_1, \\
M_{22}(\mathbf{x},\tau) &= \sum_{k=1}^{2}\int_{z_k}^{z_{k+1}} \{c_{12}^{(k)}[(z-z_{011})w_{1,1}+u_{0,1}] \\
&\quad + c_{22}^{(k)}[(z-z_{022})w_{2,2}+v_{0,2}] \\
&\quad - e_{32}^{(k)}E_3 - d_{32}^{(k)}H_3\}(z-z_{022})\,\mathrm{d}z \\
&= D_{12}w_{1,1}+G_{21}u_{0,1}+D_{22}w_{2,2}+G_{22}v_{0,2} \\
&\quad + F_{21}\psi_1+F_{22}w_{1,1}+F_{23}w_{2,2}+K_{21}\mu_1, \\
M_{12}(\mathbf{x},\tau) &= \sum_{k=1}^{2}\int_{z_k}^{z_{k+1}} \{c_{66}^{(k)}[(z-z_{012})(w_{1,2}+w_{2,1}) \\
&\quad + u_{0,2}+v_{0,1}]\}(z-z_{012})\,\mathrm{d}z \\
&= \Delta_{11}(w_{1,2}+w_{2,1})+\Gamma_{11}(u_{0,2}+v_{0,1}), \\
Q_1(\mathbf{x},\tau) &= \kappa\sum_{k=1}^{2}\int_{z_k}^{z_{k+1}} c_{55}^{(k)}(w_1+w_{3,1})\,\mathrm{d}z \\
&= C_1(w_1+w_{3,1}), \\
Q_2(\mathbf{x},\tau) &= \kappa\sum_{k=1}^{2}\int_{z_k}^{z_{k+1}} c_{44}^{(k)}(w_2+w_{3,2})\,\mathrm{d}z \\
&= C_2(w_2+w_{3,2}), \\
N_{11}(\mathbf{x},\tau) &= \sum_{k=1}^{2}\int_{z_k}^{z_{k+1}} \{c_{11}^{(k)}[(z-z_{011})w_{1,1}+u_{0,1}] \\
&\quad + c_{12}^{(k)}[(z-z_{022})w_{2,2}+v_{0,2}] - e_{31}^{(k)}E_3 - d_{31}^{(k)}H_3\}\,\mathrm{d}z \\
&= G_{11}w_{1,1}+P_{11}u_{0,1}+G_{21}w_{2,2}+P_{12}v_{0,2} \\
&\quad + S_{11}\psi_1+S_{12}w_{1,1}+S_{13}w_{2,2}+J_{11}\mu_1, \\
N_{22}(\mathbf{x},\tau) &= \sum_{k=1}^{2}\int_{z_k}^{z_{k+1}} \{c_{12}^{(k)}[(z-z_{011})w_{1,1}+u_{0,1}] \\
&\quad + c_{22}^{(k)}[(z-z_{022})w_{2,2}+v_{0,2}] - e_{32}^{(k)}E_3 - d_{32}^{(k)}H_3\}\,\mathrm{d}z \\
&= G_{12}w_{1,1}+P_{12}u_{0,1}+G_{22}w_{2,2}+P_{22}v_{0,2} \\
&\quad + S_{21}\psi_1+S_{23}w_{1,1}+S_{22}w_{2,2}+J_{21}\mu_1, \\
N_{12}(\mathbf{x},\tau) &= \sum_{k=1}^{2}\int_{z_k}^{z_{k+1}} \{c_{66}^{(k)}[(z-z_{012})(w_{1,2}+w_{2,1}) \\
&\quad + u_{0,2}+v_{0,1}]\}\,\mathrm{d}z \\
&= \Gamma_{11}(w_{1,2}+w_{2,1})+\Gamma_{21}(u_{0,2}+v_{0,1}),
\end{aligned}
\tag{A.1}
$$

where

$$
\begin{aligned}
D_{11} &= \sum_{k=1}^{2} c_{11b}^{(k)}[\tfrac{1}{3}(z_{k+1}^3-z_k^3) \\
&\quad - z_{011}(z_{k+1}^2-z_k^2)+z_{011}^2(z_{k+1}-z_k)] \\
&\quad + (c_{11t}^{(1)}-c_{11b}^{(1)})\left(\frac{h_1^3}{4}-2z_{011}\frac{h_1^2}{3}-z_{011}^2\frac{h_1}{2}\right), \\
D_{22} &= \sum_{k=1}^{2} c_{22b}^{(k)}[\tfrac{1}{3}(z_{k+1}^3-z_k^3) \\
&\quad - z_{022}(z_{k+1}^2-z_k^2)+z_{022}^2(z_{k+1}-z_k)] \\
&\quad + (c_{22t}^{(1)}-c_{22b}^{(1)})\left(\frac{h_1^3}{4}-2z_{022}\frac{h_1^2}{3}-z_{022}^2\frac{h_1}{2}\right),
\end{aligned}
$$

$$D_{12} = \sum_{k=1}^{2} c_{12b}^{(k)}[\tfrac{1}{3}(z_{k+1}^3 - z_k^3) - (z_{011}+z_{022})\tfrac{1}{2}(z_{k+1}^2 - z_k^2) + z_{011}z_{022}(z_{k+1}-z_k)] + (c_{12t}^{(1)} - c_{12b}^{(1)})\left(\frac{h_1^3}{4} - (z_{011}+z_{022})\frac{h_1^2}{3} - z_{011}z_{022}\frac{h_1}{2}\right),$$

$$\Delta_{11} = \sum_{k=1}^{2} c_{66b}^{(k)}[\tfrac{1}{3}(z_{k+1}^3 - z_k^3) - z_{012}(z_{k+1}^2 - z_k^2) + z_{012}^2(z_{k+1}-z_k)] + (c_{66t}^{(1)} - c_{66b}^{(1)})\left(\frac{h_1^3}{4} - 2z_{012}\frac{h_1^2}{3} - z_{012}^2\frac{h_1}{2}\right),$$

$$G_{11} = \sum_{k=1}^{2} c_{11b}^{(k)}[\tfrac{1}{2}(z_{k+1}^2 - z_k^2) - z_{011}(z_{k+1}-z_k)] + (c_{11b}^{(1)} - c_{11b}^{(1)})\left(\frac{h_1^2}{3} - z_{011}\frac{h_1}{2}\right),$$

$$G_{12} = \sum_{k=1}^{2} c_{12b}^{(k)}[\tfrac{1}{2}(z_{k+1}^2 - z_k^2) - z_{011}(z_{k+1}-z_k)] + (c_{12b}^{(1)} - c_{12b}^{(1)})\left(\frac{h_1^2}{3} - z_{011}\frac{h_1}{2}\right),$$

$$G_{21} = \sum_{k=1}^{2} c_{12b}^{(k)}[\tfrac{1}{2}(z_{k+1}^2 - z_k^2) - z_{022}(z_{k+1}-z_k)] + (c_{12b}^{(1)} - c_{12b}^{(1)})\left(\frac{h_1^2}{3} - z_{022}\frac{h_1}{2}\right),$$

$$G_{22} = \sum_{k=1}^{2} c_{22b}^{(k)}[\tfrac{1}{2}(z_{k+1}^2 - z_k^2) - z_{022}(z_{k+1}-z_k)] + (c_{22b}^{(1)} - c_{22b}^{(1)})\left(\frac{h_1^2}{3} - z_{022}\frac{h_1}{2}\right),$$

$$\Gamma_{11} = \sum_{k=1}^{2} c_{66b}^{(k)}[\tfrac{1}{2}(z_{k+1}^2 - z_k^2) - z_{012}(z_{k+1}-z_k)] + (c_{66b}^{(1)} - c_{66b}^{(1)})\left(\frac{h_1^2}{3} - z_{012}\frac{h_1}{2}\right),$$

$$\Gamma_{21} = \sum_{k=1}^{2} c_{66b}^{(k)}(z_{k+1}-z_k) + (c_{66t}^{(1)} - c_{66b}^{(1)})\frac{h_1}{2},$$

$$F_{11} = \sum_{k=1}^{N} e_{31}^{(k)}\frac{1}{z_{k+1}-z_k}\left[\frac{1}{2}(z_{k+1}^2 - z_k^2) - z_{011}(z_{k+1}-z_k)\right],$$

$$F_{12} = \frac{e_{31}(\alpha_{33}d_{31} - e_{31}\gamma_{33}) + d_{31}(e_{31}\alpha_{33} - d_{31}h_{33})}{(\alpha_{33}\alpha_{33} - \gamma_{33}h_{33})} \times \left[\frac{h^3 - h_1^3}{3} - (z_{011}+z_2)\frac{h^2 - h_1^2}{2} + z_{011}z_2h_2\right],$$

$$F_{13} = \frac{e_{31}(\alpha_{33}d_{32} - e_{32}\gamma_{33}) + d_{31}(e_{32}\alpha_{33} - d_{32}h_{33})}{(\alpha_{33}\alpha_{33} - \gamma_{33}h_{33})} \times \left[\frac{h^3 - h_1^3}{3} - (z_{011}+z_2)\frac{h^2 - h_1^2}{2} + z_{011}z_2h_2\right],$$

$$F_{21} = \sum_{k=1}^{N} e_{32}^{(k)}\frac{1}{z_{k+1}-z_k}\left[\frac{1}{2}(z_{k+1}^2 - z_k^2) - z_{022}(z_{k+1}-z_k)\right],$$

$$F_{22} = \frac{e_{32}(\alpha_{33}d_{31} - e_{31}\gamma_{33}) + d_{32}(e_{31}\alpha_{33} - d_{31}h_{33})}{(\alpha_{33}\alpha_{33} - \gamma_{33}h_{33})} \times \left[\frac{h^3 - h_1^3}{3} - (z_{022}+z_2)\frac{h^2 - h_1^2}{2} + z_{022}z_2h_2\right],$$

$$F_{23} = \frac{e_{32}(\alpha_{33}d_{32} - e_{32}\gamma_{33}) + d_{32}(e_{32}\alpha_{33} - d_{32}h_{33})}{(\alpha_{33}\alpha_{33} - \gamma_{33}h_{33})} \times \left[\frac{h^3 - h_1^3}{3} - (z_{022}+z_2)\frac{h^2 - h_1^2}{2} + z_{022}z_2h_2\right],$$

$$C_1 = \kappa\left[c_{55b}^{(1)}h_1 + (c_{55t}^{(1)} - c_{55b}^{(1)})\frac{h_1}{2} + c_{55}^{(2)}h_2\right],$$

$$C_2 = \kappa\left[c_{44b}^{(1)}h_1 + (c_{44t}^{(1)} - c_{44b}^{(1)})\frac{h_1}{2} + c_{44}^{(2)}h_2\right],$$

$$P_{11} = c_{11b}^{(1)}h_1 + c_{11}^{(2)}h_2 + (c_{11t}^{(1)} - c_{11b}^{(1)})\frac{h_1}{2},$$

$$P_{12} = c_{12b}^{(1)}h_1 + c_{12}^{(2)}h_2 + (c_{12t}^{(1)} - c_{12b}^{(1)})\frac{h_1}{2},$$

$$P_{22} = c_{22b}^{(1)}h_1 + c_{22}^{(2)}h_2 + (c_{22t}^{(1)} - c_{22b}^{(1)})\frac{h_1}{2},$$

$$S_{11} = \sum_{k=1}^{2} e_{31}^{(k)}, \qquad S_{21} = \sum_{k=1}^{2} e_{32}^{(k)},$$

$$J_{11} = \sum_{k=1}^{2} d_{31}^{(k)}, \qquad J_{21} = \sum_{k=1}^{2} d_{32}^{(k)},$$

$$S_{12} = \frac{e_{31}(\alpha_{33}d_{31} - e_{31}\gamma_{33}) + d_{31}(e_{31}\alpha_{33} - d_{31}h_{33})}{(\alpha_{33}\alpha_{33} - \gamma_{33}h_{33})} \times \left[\frac{h^2 - h_1^2}{2} + z_2h_2\right],$$

$$S_{13} = \frac{e_{31}(\alpha_{33}d_{32} - e_{32}\gamma_{33}) + d_{31}(e_{32}\alpha_{33} - d_{32}h_{33})}{(\alpha_{33}\alpha_{33} - \gamma_{33}h_{33})} \times \left[\frac{h^2 - h_1^2}{2} + z_2h_2\right],$$

$$S_{23} = \frac{e_{32}(\alpha_{33}d_{31} - e_{31}\gamma_{33}) + d_{32}(e_{31}\alpha_{33} - d_{31}h_{33})}{(\alpha_{33}\alpha_{33} - \gamma_{33}h_{33})} \times \left[\frac{h^2 - h_1^2}{2} + z_2h_2\right],$$

$$S_{22} = \frac{e_{32}(\alpha_{33}d_{32} - e_{32}\gamma_{33}) + d_{32}(e_{32}\alpha_{33} - d_{32}h_{33})}{(\alpha_{33}\alpha_{33} - \gamma_{33}h_{33})} \times \left[\frac{h^2 - h_1^2}{2} + z_2h_2\right]. \tag{A.2}$$

Appendix B. List of notations

B_i	Magnetic induction
$c_{\alpha\beta}^{(i)}$	Corresponding material parameters for ith layer
$c_{\alpha\beta b}^{(i)}$	Corresponding to material parameters on the bottom surfaces for ith layer
$c_{\alpha\beta t}^{(i)}$	Corresponding to material parameters on top surfaces for ith layer
c_{ijkl}	Elasticity coefficients
D_i	Electrical displacement vector
d_{ijk}	Piezomagnetic coefficients
e_{ijk}	Piezoelectric coefficients
E_i	Electric field vector
$f_{,i}$	Partial derivative of the function f
$\dot{f}$	Time derivative of the function f
$\tilde{f}$	Prescribed value of the function f
h	Total thickness of plate
h_1	Thickness of the FGM plate
h_2	Thickness of MEE layer
h_{ij}	Dielectric permittivities
H_i	Magnetic intensity vector
I_M, I_Q	Global inertial characteristics of the laminate plate
$M_{\alpha\beta}$	Bending moments
n_α	Unit outward normal vector to the boundary $\partial\Omega_s^i$
$N_{\alpha\beta}$	Normal stresses
q, (q_α)	(in-plane) transversal load
Q_α	Shear forces
u^h	Field variable
$\hat{u}^a$	Fictitious parameters for the approximated field variable
u_0, v_0	In-plane displacement
u_i	Displacement vector
w^a	Weight function
w_i	Rotations around x_i
$w_{\alpha\beta}^*$, w^*	Weight or test functions
z_2	Position of interference between FGM and MEE layers
z_3	Position of top surface of plate
z_{0ij}	Position of neutral plane
α_{ij}	Magnetoelectric coefficients
γ_{ij}	Magnetic permeabilities
Γ_{sM}^i	Boundary with prescribed bending moments
Γ_{sN}^i	Boundary with prescribed traction vector
Γ_{sw}^i	Boundary with prescribed rotations or displacements
Γ_{su}^i	Boundary with prescribed in-plane displacements
ε_{ij}	Strain tensor
κ	Coefficient for Reissner plate theory
μ	Magnetic potential
σ_{ij}	Stress tensor
τ	Time
$\Delta\tau$	Time step
ϕ^a	Shape function
ψ	Electric potential
Ω	Global domain
Ω_s	Local subdomain
$\partial\Omega_s^i$	Boundary of the local subdomain

References

[1] Mitchell J A and Reddy J N 1995 A refined hybrid plate theory for composite laminates with piezoelectric laminae *Int. J. Solids Struct.* **32** 2345–67

[2] Batra R C and Liang X Q 1997 The vibration of a rectangular laminated elastic plate with embedded piezoelectric sensors and actuators *Comput. Struct.* **63** 203–16

[3] Pietrzakowski M 2008 Piezoelectric control of composite plate vibration: effect of electric potential distribution *Comput. Struct.* **86** 948–54

[4] Bhargava A, Chaudhry Z, Liang C and Rogers A C 1995 Experimental verification of optimum actuator location and configuration based on actuator power factor *J. Intell. Mater. Struct.* **6** 411–8

[5] Batra R C, Liang X Q and Yang J S 1996 Shape control of vibrating simply supported rectangular plates *AIAA J.* **34** 116–22

[6] Irshik H 2002 A review on static and dynamic shape control of structures by piezoelectric actuation *Eng. Struct.* **24** 5–11

[7] Crawley E F and De Luis J 1987 Use of piezoelectric actuators as elements of intelligent structures *AIAA J.* **25** 1373–85

[8] Im S and Atluri S N 1989 Effects of a piezo-actuator on a finely deformed beam subjected to general loading *AIAA J.* **27** 1801–7

[9] Thornburgh R P and Chattopadhyay A 2001 Nonlinear actuation of smart composite using a coupled piezoelectric-mechanical model *Smart Mater. Struct.* **10** 743–9

[10] Pradhan S C 2005 Vibration suppression of FGM shells using embedded magnetostrictive layers *Int. J. Solids Struct.* **42** 2465–88

[11] Krishna Murty A V, Anjanappa M and Wu Y F 1997 The use of magnetostrictive particle actuators for vibration attenuation of flexible beams *J. Sound Vib.* **206** 133–49

[12] Friedmann P P, Carman G P and Millott T A 2001 Magnetostrictively actuated control flaps for vibration reduction in helicopter rotors—design considerations for implementation *Math. Comput. Modelling* **33** 1203–17

[13] Pan E 2001 Exact solution for simply supported and multilayered magneto-electro-elastic plates *ASME J. Appl. Mech.* **68** 608–18

[14] Pan E and Heyliger R P 2002 Free vibration of simply supported and multilayered magneto-electro-elastic plates *J. Sound Vib.* **252** 429–42

[15] Wang X and Shen Y P 2002 The general solution of three-dimensional problems in magnetoelectroelastic media *Int. J. Eng. Sci.* **40** 1069–80

[16] Chen Z R, Yu S W, Meng L and Lin Y 2002 Effective properties of layered magneto-electro-elastic composites *Compos. Struct.* **57** 177–82

[17] Zheng H, Li M and He Z 2003 Active and passive magnetic constrained damping treatment *Int. J. Solids Struct.* **40** 6767–79

[18] Lage R G, Soares C M M, Soares C A M and Reddy J N 2004 Layerwise partial mixed finite element analysis of magneto-electro-elastic plates *Comput. Struct.* **82** 1293–301

[19] Miyamoto Y, Kaysser W A, Rabin B H, Kawasaki A and Ford R G 1999 *Functionally Graded Materials: Design, Processing and Applications* (Boston, MA: Kluwer Academic Publishers)

[20] Liew K M, He X Q, Ng T Y and Sivashanker S 2001 Active control of FGM plates subjected to a temperature gradient: modelling via finite element method based on FSDT *Int. J. Numer. Methods Eng.* **52** 1253–71

[21] Wen P H and Hon Y C 2007 Geometrically nonlinear analysis of Reissener–Mindlin plate by meshless computation *Comput. Model. Eng. Sci.* **21** 177–92

[22] Atluri S N and Zhu T 1998 A new meshless local Petrov–Galerkin (MLPG) approach in computational mechanics *Comput. Mech.* **22** 117–27

[23] Atluri S N, Sladek J, Sladek V and Zhu T 2000 The local boundary integral equation (LBIE) and its meshless implementation for linear elasticity *Comput. Mech.* **25** 180–98

[24] Atluri S N 2004 *The Meshless Method, (MLPG) For Domain & BIE Discretizations* (Forsyth: Tech Science Press)

[25] Han Z D and Atluri S N 2004 Meshless local Petrov–Galerkin (MLPG) approaches for solving 3D problems in elasto-statics *Comput. Model. Eng. Sci.* **6** 169–88

[26] Mikhailov S E 2002 Localized boundary-domain integral formulations for problems with variable coefficients *Eng. Anal. Bound. Elem.* **26** 681–90

[27] Vavourakis V and Polyzos D 2007 A MLPG4 (LBIE) formulation in elastostatics *Comput. Mater. Continua* **5** 185–96

[28] Cinefra M, Carrera E, Della Croce L and Chinosi C 2012 Refined shell elements for the analysis of functionally graded structures *Compos. Struct.* **94** 415–22

[29] Sladek J, Sladek V, Wen P H and Aliabadi M H 2006 Meshless local Petrov–Galerkin (MLPG) method for shear deformable shells analysis *Comput. Model. Eng. Sci.* **13** 103–19

[30] Sladek J, Sladek V, Krivacek J, Wen P H and Zhang Ch 2007 Meshless local Petrov–Galerkin (MLPG) method for Reissner–Mindlin plates under dynamic load *Comput. Methods Appl. Mech. Eng.* **196** 2681–91

[31] Long S Y and Atluri S N 2002 A meshless local Petrov Galerkin method for solving the bending problem of a thin plate *Comput. Model. Eng. Sci.* **3** 53–63

[32] Soric J, Li Q, Jarak T and Atluri S N 2004 Meshless local Petrov–Galerkin (MLPG) formulation for analysis of thick plates *Comput. Model. Eng. Sci.* **6** 349–57

[33] Houbolt J C 1950 A recurrence matrix solution for the dynamic response of elastic aircraft *J. Aeronaut. Sci.* **17** 371–6

[34] Wen P H and Aliabadi M H 2012 Analysis of functionally graded plates by meshless method: a purely analytical formulation *Eng. Anal. Bound. Elem.* **36** 639–50

[35] Nan C W 1994 Magnetoelectric effect in composites of piezoelectric and piezomagnetic phases *Phys. Rev.* B **50** 6082–8

[36] Parton V Z and Kudryavtsev B A 1988 *Electromagnetoelasticity, Piezoelectrics and Electrically Conductive Solids* (New York: Gordon and Breach)

[37] Liu M F and Chang T P 2010 Closed form expression for the vibration problem of a transversely isotropic magneto-electro-elastic plate *ASME J. Appl. Mech.* **77** 24502–10

[38] Sladek J, Sladek V, Stanak P and Zhang Ch 2010 Meshless local Petrov–Galerkin (MLPG) method for laminate plates under dynamic loading *Comput. Mater. Continua* **15** 1–25

[39] Lancaster P and Salkauskas T 1981 Surfaces generated by moving least square methods *Math. Comput.* **37** 141–58

[40] Nayroles B, Touzot G and Villon P 1992 Generalizing the finite element method: diffuse approximation and diffuse elements *Comput. Mech.* **10** 307–18

[41] Li J Y 2000 Magnetoelectroelastic multi-inclusion and inhomogeneity problems and their applications in composite materials *Int. J. Eng. Sci.* **38** 1993–2011